

AD \_\_\_\_\_

CONTRACT NUMBER DAMD17-94-C-4009

TITLE: Development of an Automated Laser System for Burn Therapy

PRINCIPAL INVESTIGATOR: John A. Parrish, M.D.

CONTRACTING ORGANIZATION: Massachusetts General Hospital  
Boston, Massachusetts 02114

REPORT DATE: May 1998

TYPE OF REPORT: Final

PREPARED FOR: U.S. Army Medical Research and Materiel Command  
Fort Detrick, Maryland 21702-5012

DISTRIBUTION STATEMENT: Approved for public release;  
distribution unlimited

The views, opinions and/or findings contained in this report are those of the author(s) and should not be construed as an official Department of the Army position, policy or decision unless so designated by other documentation.

**DFIC QUALITY INSPECTED 2**

REPORT DOCUMENTATION PAGE			Form Approved OMB No. 0704-0188	
<small>Public reporting burden for this collection of information is estimated to average 1 hour per response, including the time for reviewing instructions, searching existing data sources, gathering and maintaining the data needed, and completing and reviewing the collection of information. Send comments regarding this burden estimate or any other aspect of this collection of information, including suggestions for reducing this burden, to Washington Headquarters Services, Directorate for Information Operations and Reports, 1215 Jefferson Davis Highway, Suite 1204, Arlington, VA 22202-4302, and to the Office of Management and Budget, Paperwork Reduction Project (0704-0188), Washington, DC 20503.</small>				
1. AGENCY USE ONLY (Leave blank)	2. REPORT DATE May 1998	3. REPORT TYPE AND DATES COVERED Final (7 Mar 94 - 31 Mar 98)		
4. TITLE AND SUBTITLE Development of an Automated Laser System for Burn Therapy		5. FUNDING NUMBERS DAMD17-94-C-4009		
6. AUTHOR(S) Parrish, John A., M.D.				
7. PERFORMING ORGANIZATION NAME(S) AND ADDRESS(ES) Massachusetts General Hospital Boston, Massachusetts 02114		8. PERFORMING ORGANIZATION REPORT NUMBER		
9. SPONSORING / MONITORING AGENCY NAME(S) AND ADDRESS(ES) U.S. Army Medical Research and Materiel Command Fort Detrick, Maryland 21702-5012		10. SPONSORING / MONITORING AGENCY REPORT NUMBER		
11. SUPPLEMENTARY NOTES				
12a. DISTRIBUTION / AVAILABILITY STATEMENT Approved for public release; distribution unlimited		12b. DISTRIBUTION CODE		
13. ABSTRACT (Maximum 200 words) <p>Substantial progress was made in the development of a diagnostic system capable of assessing the extent of burn injury and a laser-based debridement system that rapidly, precisely and bloodlessly removes burn eschar under automatic feedback control. An ICG fluorescence imager was constructed and shown to be successful in assessing burn depths in small and large animals. The distribution of ICG into burns and normal tissue was also studied supporting steps in deriving segmentation algorithms. The technique was also safely used in a pilot clinical trial. Laser speckle was evaluated successfully in a Teflon phantom mimicking burns and more recently in porcine skin burns. A laser burn debridement system was constructed and tested on porcine skin burns. Burns were tangentially excised bloodlessly and equivalent percent engraftment rates and Vancouver scar scores were obtained from laser debrided sites and sharply excised controls. Progress has been made in developing a feedback control mechanism for controlling the laser debridement system. Identifying the transition zone between burn eschar and underlying healthy tissue appears possible using reflectance spectroscopy. Finally, a more elegant laser debridement burn diagnostic robotic system has been designed via a cooperative research agreement with Sandia National laboratories.</p>				
14. SUBJECT TERMS  laser, burn injury, fluorescence, feedback control, diagnosis, debridement		15. NUMBER OF PAGES 66		16. PRICE CODE
17. SECURITY CLASSIFICATION OF REPORT Unclassified	18. SECURITY CLASSIFICATION OF THIS PAGE Unclassified	19. SECURITY CLASSIFICATION OF ABSTRACT Unclassified	20. LIMITATION OF ABSTRACT Unlimited	

19990216182

## FOREWORD

Opinions, interpretations, conclusions and recommendations are those of the author and are not necessarily endorsed by the U.S. Army.

\_\_\_\_ Where copyrighted material is quoted, permission has been obtained to use such material.

\_\_\_\_ Where material from documents designated for limited distribution is quoted, permission has been obtained to use the material.

SP Citations of commercial organizations and trade names in this report do not constitute an official Department of Army endorsement or approval of the products or services of these organizations.

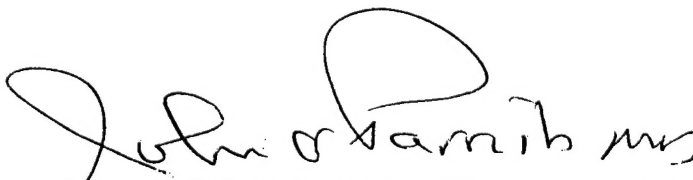
P In conducting research using animals, the investigator(s) adhered to the "Guide for the Care and Use of Laboratory Animals," prepared by the Committee on Care and Use of Laboratory Animals of the Institute of Laboratory Resources, National Research Council (NIH Publication No. 86-23, Revised 1985).

A For the protection of human subjects, the investigator(s) adhered to policies of applicable Federal Law 45 CFR 46.

\_\_\_\_ In conducting research utilizing recombinant DNA technology, the investigator(s) adhered to current guidelines promulgated by the National Institutes of Health.

\_\_\_\_ In the conduct of research utilizing recombinant DNA, the investigator(s) adhered to the NIH Guidelines for Research Involving Recombinant DNA Molecules.

\_\_\_\_ In the conduct of research involving hazardous organisms, the investigator(s) adhered to the CDC-NIH Guide for Biosafety in Microbiological and Biomedical Laboratories.

  
\_\_\_\_  
PI - Signature Date

## TABLE OF CONTENTS

FRONT COVER_____	i
REPORT DOCUMENTATION PAGE (SF 298)_____	ii
FOREWORD_____	iii
TABLE OF CONTENT_____	iv
INTRODUCTION_____	1
BODY	
I. BURN DIAGNOSTIC SYSTEM_____	4
1. TESTING THE PROTOTYPE_____	5
2. SEGMENTATION AND ANALYSIS ALGORITHMS_____	6
3. DETERMINING EFFICACY IN ADIPOSE TISSUE_____	9
4. PARTITIONING OF INDOCYANINE GREEN_____	9
5. ALTERNATE OPTICAL SCHEMES_____	15
II. LASER DEBRIDEMENT SYSTEM_____	22
1. FORMULATE DESIGN CRITERIA_____	22
2. CONSTRUCT PROTOTYPE SYSTEM_____	22
3. TEST SYSTEM IN ANIMALS_____	24
4. OPTIMIZE LASER ABLATION PROCESS_____	30
5. EXAMINE VARIOUS FEEDBACK MECHANISM_____	32
6. FAMILIARIZE MEDICAL PERSONNEL_____	35
7. CONSTRUCT A SECOND PROTOTYPE_____	36
CONCLUSIONS_____	37
REFERENCES_____	38
BIBLIOGRAPHY	
PERSONNEL_____	44
PUBLICATIONS_____	45
MEETING ABSTRACT_____	46
APPENDICES	
A. BURN DIAGNOSTIC SYSTEM TECHNICAL SPECS._____	A1
B. LASER DEBRIDEMENT SYSTEM TECHNICAL SPECS._____	B1



## INTRODUCTION

Greater than 10% of wartime casualties are the direct result of burn injury. In addition, there are more than 100,000 serious civilian burn injuries per year in the United States which result in millions of hospital days and an estimated cost of several billion dollars. Thus, a method to improve the clinical outcome of burn victims would represent an important medical advance. Burn surgery has made tremendous progress by providing aggressive supportive care for burn victims and by performing excision and skin-grafting of deep partial and full thickness burns in a timely fashion. The two major limitations of this modern approach to burn management are bleeding during burn eschar debridement and an inability to accurately determine depth of burn injury. The ultimate goal of our investigations is to develop an integrated laser-based system that would overcome both of these limitations. The system will determine the extent of burn injury and automatically debride burn eschar in a rapid, hemostatic fashion under feedback control. Furthermore, the system will produce an ablation bed suitable for subsequent skin grafting by conventional skin grafts or cultured autologous keratinocytes. Therefore, when fully implemented this system would represent a major advance in the care of burn victims. In addition, it is likely that the system will contribute to the management of other conditions requiring debridement and skin grafting such as chemical and biological agents, skin tumors, cold (frostbite) injury and skin ulcers. The ultimate goal of this multi-year research program was to develop two systems to assist the burn surgeon in caring for patients with burn trauma. The first system is a diagnostic system capable of assessing the extent of burn injury including an accurate determination of burn depth. The second system is a laser-based debridement system in which a high power laser is used to rapidly, precisely and bloodlessly remove burned tissue under automatic feedback control ("laser robot"). A prototype diagnostic system was constructed in the first phase of this project which was funded by DOD (Grant #DAMD-17-92-J-2019). In this report, we describe further refinements to the diagnostic system with further tests in porcine skin burns and human burns. In addition a prototype laser debridement system was constructed and tested in porcine skin burns.

Prompt burn eschar excision with immediate wound closure decreases mortality and shortens hospital stay and is the standard of care in most institutions [Tompkins, 1987; Cope 1947]. Ideally, excision of burned skin occurs as soon as possible after admission, once the patient is hemodynamically stable [Demling, 1989]. In order to conserve surface and subjacent skin during surgery, areas of skin which will heal spontaneously with minimal scarring (superficial dermal or partial thickness burns) must be differentiated from areas which will not heal within two weeks and therefore require surgical excision and grafting (deep dermal or full thickness burns) [Demling, 1989; Jackson, 1970b; MacMillan, 1979]. Clinical criteria to distinguish burn depth including sensitivity to pin-prick, visual appearance and viable cutaneous circulation are often inaccurate in predicting the depth of a burn wound [Jackson, 1970a] and in guiding surgeons during excisions [Hauben, 1979]. When conservative tangential excisions are performed in the primary excision and grafting of wounds, the surgeon uses punctate capillary bleeding to delineate underlying viable tissue but this results in significant blood loss [Demling, 1989; Janzekovic, 1970; Jackson, 1972]. Once within a burn or escharotomy site, clinical criteria can not reliably identify the critical zone of vascular stasis which divides necrotic from viable tissue [Hauben, 1979; Jackson, 1982; Groves, 1971; Jackson, 1969; Jackson, 1973]. It is often easier to excise the entire burned skin and subcutaneous tissue to muscle fascia, which is a distinct, graftable plane [Demling, 1989; Levine, 1978] but this approach may sacrifice significant amounts of viable skin. Thus, the accurate determination of burn depth is a key component of modern burn surgery and a method to remove eschar without bleeding would significantly reduce operative morbidity.

Because clinical assessment of burn depth is difficult, several attempts to develop technical means of predicting burn depth have been made during the last half-century. Unfortunately, none have gained widespread clinical acceptance. Limitations have included inadequate accuracy on selected days post-burn, cumbersome and time consuming techniques and toxicity. Passive infrared thermography showed early promise in distinguishing burn depth [Mladick, 1966; Newman, 1980; Cole, 1990; Barnes, 1963] but false positive images were common and thermography has not been able to reproducibly distinguish superficial from deep-dermal burns. High frequency ultrasound was felt capable of delineating the acoustic interface between viable and necrotic skin [Kalus, 1979; Cantrell, 1984; Wachtel, 1986; Bauer, 1989] but when tested clinically could not exceed the ability of burn surgeons to gauge burn depth by clinical methods [Kalus, 1979]. Burn wound depth has also been evaluated by the use of radioactive isotopes [Bennett, 1957] where re-epithelialization and hypercellularity increase isotope uptake in a healing area. This too has not proven to be a clinically viable technique. An

optical reflectance technique has been used to evaluate debrided burn injuries [Afromowitz, 1987; Afromowitz, 1988]. The ratios of reflected green and red light to infrared light were determined initially with a fiberoptic instrument and later with a video camera. In clinical testing, the best correlation between reflectance ratio values and burn depth occurred on day three post-burn in areas where the epidermis was removed. The major limitation of this technique is its inaccuracy in the crucially important first three days following burn injury. Blood flow measurements using the Doppler technique have been used to estimate the depth of burn injury in human skin [Michaels, 1984; Waxman, 1989]. Although accurate, the method is slow (measurement at a single point requires 10-15 minutes) and can not provide information over a large area burn.

In this report we describe a fluorescence technique to assess burn depth. The use of fluorescent vital dyes to detect viable cutaneous circulation and predict burn depth is not new. In 1943, intravenous fluorescein was used to differentiate second from third-degree burns [Dingwall, 1943]. It was hypothesized that the tissue destruction present in a third-degree burn impeded vascular transportation of the drug to the upper layers of burned skin. Studies on medical student volunteers who received injections of fluorescein demonstrated that when examined with a Woods lamp "third-degree" burns appeared black, while "second-degree" burns appeared yellow-green. The observed fluorescence intensity was dependent on two physical factors; a viable cutaneous circulation which transported the dye to the tissue and overlying burn eschar which transmitted, absorbed and scattered the incident exciting Woods lamp (ultraviolet) radiation and subsequent fluorescence emission (560 nm). The shallow (approximately 50  $\mu$ m) penetration of incident ultraviolet light through skin and eschar [Anderson, 1981] limited this method to evaluating intact superficial cutaneous circulation and deeper viable remnants of burned skin covered with eschar could not be detected. It therefore failed to differentiate superficial from deep partial thickness wounds and did not gain clinical acceptance.

In 1983, another attempt to use intravenous fluorescein for burn depth assessment was made with a fluorometer to quantify fluorescence [Gatti, 1983]. Quantitative fluorescence measurements during the first 48 hours and between 72 and 144 hours post burn were able to distinguish partial thickness from full thickness burns. Partial thickness burns exhibited fluorescence within 10 minutes after intravenous injection of fluorescein while full thickness burns showed negligible fluorescence. However, the method failed to distinguish between shallow and deep partial thickness burns, which in many institutions require different surgical approaches [Demling, 1989].

In our approach, indocyanine green (ICG) is used as the fluorescent probe. ICG is a tricarboyanine dye that has been used for measuring cardiac and hepatic output in humans for thirty years [Fox, 1956; Rapaport, 1959]. It is nontoxic and rapidly excreted by the liver into bile [Cherrick, 1960]. ICG has several advantages over fluorescein for assessing cutaneous blood volume/perfusion and burn depth. Unlike fluorescein which has a single UV absorption band and a mid-visible fluorescence emission, ICG has two major absorption bands, one in the near-UV and one in the near-IR and produces infrared (840 nm) fluorescence. Because near-IR light travels through tissue with little absorption, ICG fluorescence emissions arising deep within tissue can be detected at the surface; something that is not possible with fluorescein. The assessment of burn depth can be viewed as a determination of viable cutaneous circulation at different levels in the skin. Because UV light penetrates skin and eschar superficially compared with near-IR light [Anderson, 1981] superficial and deep intravascular ICG can be differentiated by comparing fluorescence following UV and near-IR excitation, respectively. This can then be correlated with depth of burn injury. In addition, ICG is strongly bound to serum proteins and when compared to fluorescein (which is less than 50% protein bound), ICG is much less likely to leak from the vasculature into surrounding tissue. We have demonstrated the validity of this technique in small and large animals and a prototype system suitable for clinical use has been constructed and safely used in clinical trials.

The ideal laser for burn surgery would remove tissue precisely and efficiently, coagulate blood vessels and permit normal healing of skin and skin grafts. For over 20 years, the continuous wave carbon dioxide laser has been the most widely used laser for burn surgery [Levine, 1975]. This laser can decrease blood loss compared with electrosurgical knife or cold steel scalpel because it produces residual thermal damage on the order of 1 mm. Unfortunately, this zone of thermal damage is essentially a burn eschar and its presence greatly impedes healing, and because of poor healing, lasers have not been used widely for burn surgery. However, recent advances in the understanding of laser-tissue interactions coupled with a dramatic increase in the number of laser sources have made it possible to control the amount of laser-induced thermal damage. Our work in this

area has demonstrated that with carefully chosen laser parameters, it is possible to remove burn eschar without bleeding and yet provide a bed that does not impede subsequent graft take.

In this report we describe a research effort to integrate the two important observations described above. In particular, by using a diagnostic system to control a laser ablation system, we believe it is possible to construct a laser-based system that rapidly, accurately and bloodlessly removes burn eschar under automatic (feedback) control. Although various spectroscopic techniques were investigated, reflectance spectroscopy worked best for identifying the transition plane separating burn eschar from underlying healthy tissue. This diagnostic is currently being tested prospectively in a porcine skin burn model. The ultimate objective of this multi-year research program is to develop an integrated laser-based system for treating burn injury. When completed, the system will be capable of assessing the extent of burn injury including an accurate determination of burn depth and will rapidly debride burn eschar using a high-power laser under optical feedback control.

The specific objectives of this proposal were:

#### **I. Burn Diagnostic System**

1. Test the prototype system in burn victims
2. Develop appropriate segmentation and analysis algorithms to accurately diagnose burn depth using images obtained from clinical and animal trials
3. Determine the efficacy of the method to diagnose the depth of burn injury in adipose tissue
4. Determine the partitioning of indocyanine green within normal and burned tissue
5. Examine alternate optical schemes for improving depth definition.

#### **II. Laser Debridement System**

1. Formulate design criteria for a laser debridement system based on our preliminary data and acquire the necessary system components
2. Construct a prototype system for burn debridement
3. Test and optimize the system in animals
4. Optimize the laser ablation process by performing studies of laser ablation of skin and using theoretical models of ablation to analyze the data
5. Examine and compare various optical feedback control mechanisms including ICG fluorescence, autofluorescence and reflectance
6. Familiarize medical personnel from military and civilian hospitals in the use of the system in preparation for clinical testing
7. Construct a second prototype system for testing at a second clinical site.

Details of each objective are given in the following pages.

## I. Burn Diagnostic System

Clinical diagnosis of superficial and very deep burns is accurate during the first few days following injury but even experienced clinicians have difficulty differentiating between intermediate partial thickness burns capable of healing with minimal granulation and deeper partial thickness burns that require excision and grafting [Heimbach, 1992; Green, 1992a]. Early diagnosis of these burns would facilitate prompt excision and thereby improve patient outcome. Heimbach and coworkers have presented a thorough review summarizing a large variety of technologies for determining burn depths, but despite these efforts, clinical assessment by an experienced burn surgeon remains the standard for assessing burns today. Infrared-excited fluorescence of intravenously administered indocyanine green (ICG) (Cardio-Green, Becton Dickinson Microbiology Division, Cockeysville, MD), has been used as a method for early determination of burn depth. ICG fluorescence was shown to accurately differentiate between full thickness and partial thickness burns in rat skin [Green, 1992a]. More recent work in our laboratory using porcine skin demonstrated that the fluorescence intensity of ICG in burns can accurately predict burns that heal on their own with minimal granulation from full thickness burns independent of their location. In a clinical trial, fluorescence images of burns using low doses of indocyanine green (0.2 mg/kg body weight iv) in 10 adult patients were able to separate superficial burns from deep burns [Sheridan, 1995] and a larger trial is underway. The purpose of this study was to understand the mechanism underlying this technique. Fluorescence microscopy was used to determine the distribution of ICG in normal and burn-injured porcine skin.

A block diagram of the fluorescence imaging system is shown in Figure 1. A 2400 W-s xenon flashlamp (MW20QC, Speedotron Corp., Chicago, IL), filtered with a 10 nm bandpass filter (780BP10, Omega Optical, Inc., Brattleboro, VT) to emit 780 nm light, was used to excite ICG. The incident light fluence was 1.3 mJ/cm<sup>2</sup>. The resultant fluorescence emission at 825 nm was recorded with a CCD camera (CCD-C72, Dage-MTI Corp., Michigan City, IN) and a 20 nm bandpass filter (825BP20, Omega Optical, Inc., Brattleboro, VT). The center wavelength of the excitation bandpass filter was chosen to be slightly blue-shifted from the absorption maximum of ICG (805 nm) to minimize interference with the emission filter. The relative percent decrease in absorption between 780 nm and 805 nm is 20%. The images were captured and stored by a computer for further processing. The ratio of ICG fluorescence from the burns relative to adjacent normal tissue were determined from the images and correlated with the depth of burn injury as determined by histology (see below). The technical specifications for this system are given in Appendix A.

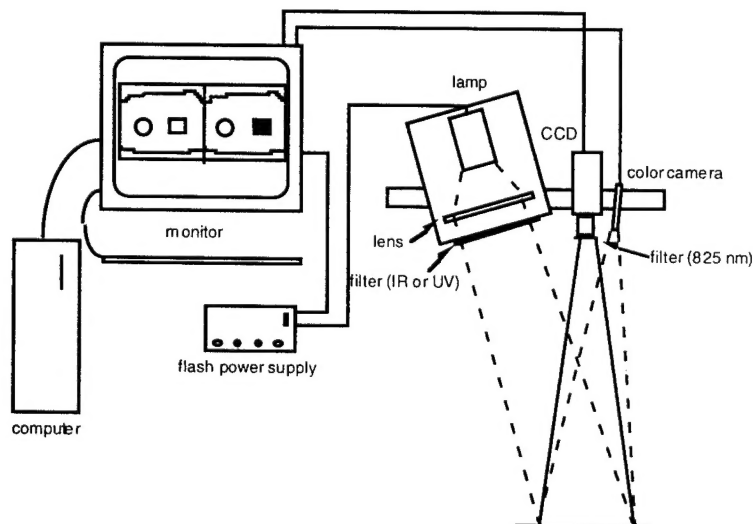


Figure 1. Schematic of the prototype burn diagnostic system including recent modification of the lamp source. The image intensifier used in some experiments is not shown.

### *1. Test the prototype system in burn victims*

The prototype burn diagnostic system was used to image Indocyanine Green (ICG) in 10 patients. All patients were male and their ages ranged between 27 to 80 years. Six patients were Caucasian, 2 African American and 1 Asian. Five burns were located on the lower extremities, 2 on the upper extremities, 1 on the back and 1 on the abdomen. The etiology of the burns were as follows: 2 from hot oil on stove, 1 each from hot water on stove, working with alkaline (pH 12) cement, clothes caught fire from cigarette, clothes caught fire from a stove paper fire, electrical shock from copper wire, flash burn from epoxying an underground gas tank, and flash burn from propane lantern. Six of the 9 patients required grafting. All patients received 0.2 mg/kg ICG intravenously and 825 nm fluorescence from ICG was imaged minutes later. Images were also taken at 1, 2, 3, 4, and 10 minutes post injection. There were no complications. Representative images of a superficial and a full thickness burn are given below (Fig 2).

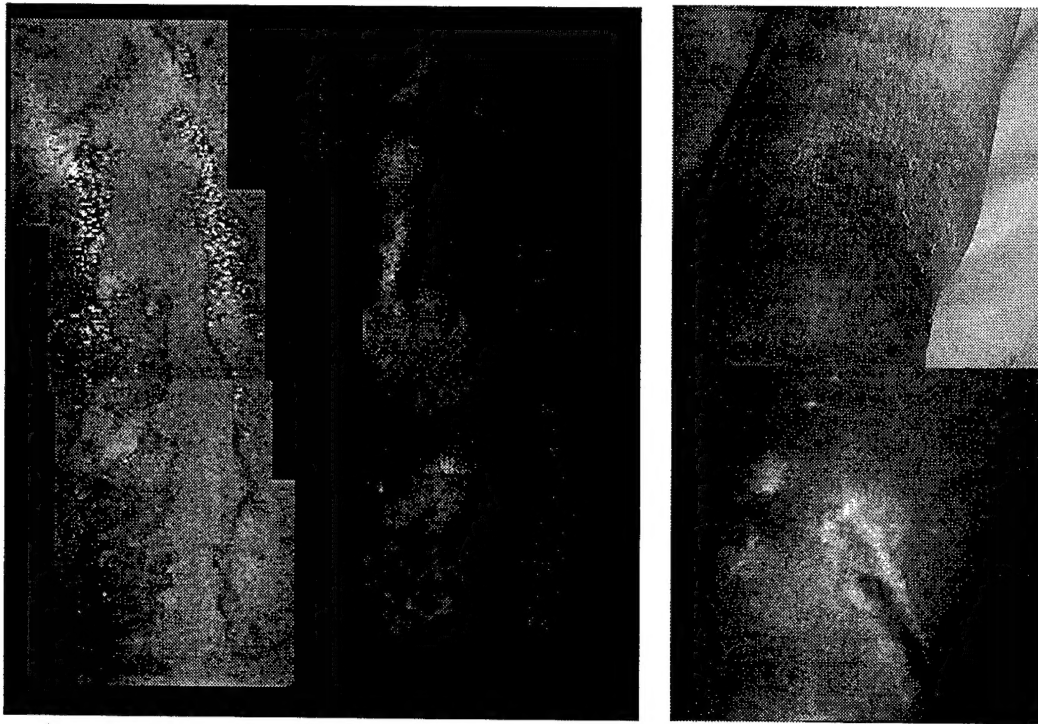


Figure 2. ICG fluorescence image of a superficial (left panel) and a deep (right panel) burn. The corresponding black and while image as also shown. Typically, the intensity of fluorescence from superficial burns is greater than surrounding normal tissue while the opposite is true for full thickness burns.

In general, images that required excision and grafting showed less fluorescence in comparison to normal tissue while superficial burns exhibited enhanced fluorescence. The ICG fluorescence intensity correlates with decreased blood flow in deep burns due to thrombosed vasculature and increased flow in superficial wound due to hyperemia and increase permeability. Although it is too early to draw any firm conclusions from this study, the main conclusions from this study are the technique is safe and the present dose (0.2 mg/kg) yields adequate signal for fluorescence images. The burn to normal tissue fluorescence contrast ratios were found from these images, but firm conclusions from this study regarding the accuracy of the technique cannot be made because of unforeseen issues discovered in this study that affect the contrast ratio. The first and major effect noticed in this study is that, unlike burned pig skin which develops thick eschar, almost all burn wounds in humans were partially debrided and had wet open wounds that lack eschar. The relative fluorescence from these areas are generally higher than normal areas because the thick eschar reduces the fluorescence seen from underlying vasculature. In addition, the melanin in normal skin decreases the observed fluorescence of ICG by absorbing at both the excitation and emission wavelengths. The burn wounds studied from Afro-American patients were wet and open and lack melanin yielding relatively higher contrast ratios.



The technology was transfer to Star Medical Technologies, Inc., Pleasanton CA through a License Agreement and further studies are underway. A second prototype device was developed by SMT that uses a high power laser diode. Preliminary results with a prototype device measuring ICG fluorescence in cuvette suggest a five-fold increase in sensitivity due to better stray light rejection. In addition, the output energy of a laser diode based system is used more efficiently compared to a filtered-lamp based system. The problems noted above concerning the effects of partial debridement and skin color on the intensity of ICG fluorescence may be resolved by comparing the pattern of ICG as it distributes into skin, a technique akin to evaluating retinal vessels using fluorescein angiography. Star Medical is further developing the technology for human studies using internal funds and a SBIR contract with the Air Force (Contract F29601-95-C-0034). To date SMT has studied 12 burn patients, 15 patients with reconstructive skin flaps and 12 patients with ulcers.

*2. Develop appropriate segmentation and analysis algorithms to accurately diagnose burn depth using images obtained from clinical and animal trials*

Segmentation and analysis algorithms are under development. Domestic farm swine (Parsons Farm, Hadley, MA) weighing 20-25 kg were used in this study. The animals were anesthetized with ketamine (20 mg/kg IM) followed by inhaled halothane (1.5%) in oxygen (4 l/min) and nitrous oxide (2 l/min). Burns were created on the skin of the animal using a heated brass block. A 4 cm x 4 cm square brass block was heated to 100°C in boiling water then held against the shaved and sterilely prepped skin of the animal to create the burn. The time of contact between the block and skin produces varying degrees of thermal injury. The time durations used in this study (4, 6, 8, and 10 s) were selected based on previous work to create burns of indeterminate depth. After photographing the wounds, all burns were covered with silver sulfadiazine 1% cream (Silvadene, Boots Pharmaceutical, Lincolnshire, IL) and sterile gauze held in place with elastic bandage and staples. The dressings were changed every 3 to 4 days. Pain medication (buprenorphine 0.3 mg IM) was provided as needed during the first week following the application of burns. Seven pigs were used in this study, each having 8 to 10 burns of varying depth and location: 3 or 4 burns in the paraspinal region (back) and flank, and 2 burns on the abdomen. The care and use of animals in this study complied with the "MGH Policies and Procedures for the Care and Use of Laboratory Animals" which follows guidelines set forth by the National Institute of Health along with other regulatory agencies. All procedures were approved by the MGH Subcommittee on Research Animal Care.

ICG fluorescence images were recorded at 1, 24, 48, or 72 hours post-burn using the prototype device shown in Figure 1. Baseline images of each burn were taken prior to the injection of ICG. ICG (0.2 mg/kg) was then injected intravenously via a lateral ear vein as a bolus flushed with 0.9% isotonic saline. Images were taken 15 minutes later. Each image acquisition sequence results in three images: a color image of the site for documentation purposes (acquired with the color camera), a background image of the site (acquired *without* the NIR flash), and a fluorescence image of the site (acquired with the NIR flash). The background image was subtracted from the corresponding fluorescence image. Next, the pre-injection fluorescence image was spatially registered to and subtracted from the post-injection fluorescence image. This resulted in an image where the fluorescence intensity scales with the amount of ICG in burn and adjacent normal tissue. The burn to normal tissue (B/N) fluorescence ratio was determined from the mean fluorescence intensity in a small (10 x 10 pixels) window within the burn site divided by the mean fluorescence intensity in adjacent normal skin. The mean burn to normal (B/N) fluorescence ratio was then determined from an average of measurements made at four different locations in the same burn.

Burns of various depths and locations were induced in skin following the procedure detailed above. The burns were imaged at 1, 24, 48, or 72 hours post-burn and then allowed to heal. Twenty-one days following the injury, an experienced burn surgeon who was blinded to the ICG fluorescence results was asked to assess whether the wounds had healed. The B/N fluorescence ratio for each burn was then compared to the final outcome. In this manner, the accuracy of the fluorescence ratio as a means of predicting healing was evaluated.

The threshold discriminant algorithm was defined following three observations noted below. First, enhanced fluorescence was shown to emit from a well-defined band of tissue consistent with the zone of hyperemia. Secondly, the intensity of this band decreased with time post-burn. And thirdly, the intensity of

ICG fluorescence measured at the surface decreased exponentially with the depth of this band. Therefore, the burn to normal fluorescence intensity ratio of ICG measured at the tissue surface can be modeled as:

$$R(t, d) = \frac{F_B(t, d)}{F_N} = \text{const} \cdot C_{ICG, B}(t) \cdot \exp(-\mu d), \quad (1)$$

where  $F_B$  and  $F_N$  are the fluorescence intensity of ICG in the burn and normal tissue and  $F_B$  is dependent on the time post burn when imaged,  $t$ , and on the depth of the burn,  $d$ . The intensity of fluorescence observed at the tissue surface is exponentially dependent on the attenuation coefficient  $\mu$  of the tissue, that is itself dependent on the effective attenuation coefficient due to the optical scattering and absorption properties of tissue at the excitation and emission wavelengths,  $\mu = \mu_{\text{eff}}(\lambda_{\text{ex}}) + \mu_{\text{eff}}(\lambda_{\text{em}})$ . Note that because  $R(t, d)$  is a ratio of burn to normal fluorescence, the expression is, to first order, independent of the intensity of the flash, injected drug dose, fluorescence quantum yield and collection geometry. The amount of ICG present in the burn,  $C_{ICG, B}(t)$ , is dependent on the time delay between the injury and when the site was imaged and can be modeled as:

$$C_{ICG, B}(t) = C_H \cdot \exp(-kt) + C_p, \quad (2)$$

where  $C_H$  correspond to the increased ICG concentration attributed to the transient hyperemic response and  $C_p$  to the static concentration attributed to tissue perfusion following the hyperemic response. The threshold ratio value for separating burns that heal from those that do not was determined by replacing  $d$  with the critical depth,  $\chi$ . Combining these equations and solving for  $R(t, d)$  after simplifying yields:

$$R(t) = c_1 + c_2 \exp(-kt), \quad (3)$$

where the constants  $c_1$  and  $c_2$  equal  $\text{const} C_p \exp(-\mu\chi)$  and  $\text{const} C_H \exp(-\mu\chi)$ , respectively.

Clinical pictures of typical burns with their corresponding fluorescence and 21 day healing images are shown in Figure 3. The figure depicts 6, 8, and 10 s burns created 72 hours earlier in the paraspinal region. The fluorescence intensity of ICG decreased with increasing burn depth even though the clinical appearance of the burns were quite similar. Intense fluorescence was observed from the 6 s burn that healed within 21 days with minimal contracture and slight hyperpigmentation. The deeper 10 s burn shows diminished fluorescence and the wound is not completely healed at 21 days and had severe contracture with noticeable granulation tissue and hyperpigmentation. The 8 s burn healed within 21 days and had slight contracture and patchy granulation tissue.

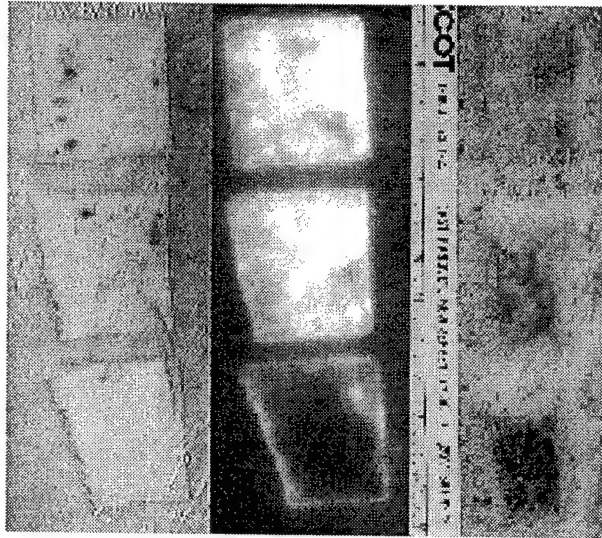


Figure 3. ICG fluorescence in burns of indeterminate depth. The clinical photos at POD #0 and 21 are shown in the left-sided and right-sided panels. The corresponding fluorescence images are shown in the middle panel. The burns going top to bottom correspond to wounds made from a heated brass block held in place for 6, 8 and 10 s. The 6 s burns was completely healed at 21 days while the 10 s burn was not and is healing from the edges of the wound with significant contracture.

The burn to normal fluorescence ratio was found from a mean of four measurements taken within the burn and nearby normal tissue. The fluorescence ratios are plotted against the age of the burn in Figure 4. Burns that healed within 21 days are plotted as open squares while burns that did not heal are plotted as open triangles. Burns that heal had a higher ratio than burns that did not heal for age matched data. However, there was no unique threshold ratio that separated the two classes independent of burn age. The solid curve in Figure 4 shows the discrimination threshold ratio that separate burns that heal within 21 days from those that do not. Using Equation 3, it is clear that this threshold ratio decreased with time delay between injury and imaging. The threshold ratio curve was calculated from a least squares fit to midpoint values determined from the lowest fluorescence ratio of the healing group and the highest fluorescence ratio from the nonhealing group. The best fit solution used  $0.59$ ,  $0.78$  and  $0.094 \text{ hr}^{-1}$  for  $c_1$ ,  $c_2$  and  $k$ , respectively.

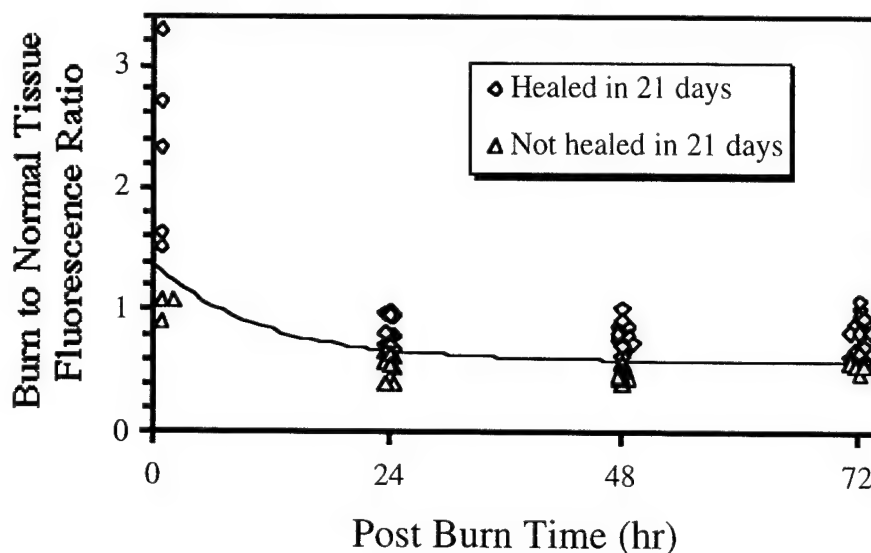


Figure 4. Burn to normal fluorescence ratio for wounds which healed or did not heal in 21 days versus time post-burn.

This study demonstrates that distinguishing burns that spontaneously heal within 21 days with minimal scarring from burns that require longer times and result in excess granulation tissue is possible using ICG fluorescence. The burn to normal tissue fluorescence ratio of intravenous ICG can be used to discriminate burns that heal within 21 days from burns that do not as long as the time that has elapsed between burn injury and imaging is known. Using a simplistic model, all sites were correctly classified as to whether they would heal or not in 21 days. The model assumes that the critical burn depth determining whether a burn will spontaneously heal within 21 days does not vary with the age of the burn.

The intensity of ICG fluorescence is greater for superficial burns when compared to deeper burns. This effect was observed consistently in burns on rat [Green, 1992a], swine [Jerath, in prep] and human [Sheridan, 1995] skin. From fluorescence microscopy studies of frozen porcine skin biopsies, the enhanced fluorescence originates from a zone of hyperemic vasculature located between the burn eschar and underlying healthy tissue [Schomacker, 1997]. The decreased fluorescence was attributed to occluded vasculature within the upper layers of burn eschar that reduced the ICG fluorescence signal recorded from patent vessels within deeper layers. The effect was first proposed from observations of fluorescein fluorescence in animals and humans [Dingwall, 1943]. The intent of our work was to show that ICG fluorescence can accurately diagnose burns that would benefit from early excision using healing as the endpoint.

ICG fluorescence is enhanced during the first 24 hours following a burn and tapers to a steady state between 24 and 72 hours. This decrease in fluorescence ratio with the age of the burn is dependent on many



factors. First as the burn wound evolves, more tissue becomes necrotic and the hyperemic zone shifts deeper into tissue [Schomacker, 1997]. The increase in eschar thickness cannot explain the entire difference, however, as two-times more fluorescence was observed for 1 hour old burns compared to 48 and 72 hour old burns when comparing burns of similar depths. This two-fold enhanced fluorescence seen in new burns was attributed to a transient hyperemic response to the injury with a concomitant increase in vascular permeability [Green, 1992a; Schomacker, 1997]. As a result, more ICG is delivered to and leaks into surrounding tissue of newly placed burns.

In conclusion, fluorescence from intravascularly administered ICG appears to be a reliable method for distinguishing thermal burns that heal in 21 days from burns that do not. However, because porcine and human skin differ, the threshold fluorescence ratios may need to be calibrated in humans where the threshold values are likely to be different. Finally, although this technique was evaluated on thermal burns, it is likely to be just as effective in evaluating cold injuries and chemical burns as well as the viability of skin grafts and flaps during reconstruction surgery.

### *3. Determine the efficacy of the method to diagnose the depth of burn injury in adipose tissue*

The objective was to diagnosing the depth of burn injury in adipose tissue during tangential excisions as an aid in determining healthy adipose tissue suitable to grafting. Although the original proposal described this objective as a separate item, in retrospect it seems obvious to fold into section II.5 below. Hence details of this work are given there.

### *4. Determine the partitioning of indocyanine green within normal and burned tissue*

Twenty-five to 35 kg farm swine (Parson's Farm, Hadley, MA) were used for this study. Burns were created 1, 24 or 48 hr prior to fluorescence imaging. The animals were placed under general anesthesia for all procedures. Animals were sedated with ketamine (20 mg/kg IM) prior to transferring to the operating room. The animal then inhaled halothane (2-3 %) with oxygen (4 l/min) and nitrous oxide (2 l/min). After induction, the rate of halothane was decreased to 1 to 1.5% as tolerated. The heart rate and peripheral oxygen saturation were monitored throughout the procedure.

Once anesthetized, the paraspinal region was clipped with electric shears, cleansed with povidone iodine, rinsed with sterile phosphate buffered salt (PBS) solution, then draped in a sterile fashion. Typically three or four burns of varying depths were created using a 4 cm x 4 cm x 2.5 cm (l x w x h) brass block preheated to 100°C in boiling water and held in place on the skin for 3, 7, 12 or 20 s. After 15 min, the wounds were covered with a layer of silver sulfadiazine 1% cream, a layer of petrolatum dressing (Xeroform, Sherwood Medical, St. Louis, MO), a layer of gauze fluff and elastic mesh, held in place with surgical staples. Prior to awakening, buprenorphine (0.3 mg IM) was given for pain management.

Twenty-four or 48 hours later, the animal was reanesthetized, the dressing removed, and the wounds cleaned with povidone iodine followed by sterile PBS. An appropriate area on the contralateral side was then prepped as before and an additional 3 or 4 burns were placed, using the same technique described above. One hour later Indocyanine Green (ICG) was administered intravenously. An injectable ICG (Cardio-Green, Becton Dickinson Microbiology Division, Cockeysville, MD) solution (5 mg/ml) was prepared and a dose of 1.0 mg/kg was given. One animal received 4.4 mg/kg to improve the contrast of the 20 s fluorescence micrographs. Similarly, because ICG could not be detected in the 20 s fluorescence micrographs at a dose of 1.0 mg/kg, the 20 s burns were omitted from the Pigs 2, 3, and 4. Fluorescence images were recorded from all burn sites immediately prior to and 15 minutes after the ICG injection. A block diagram of the fluorescence imaging system is shown in Figure 1. The images were captured and stored by a computer for further processing. The ratio of ICG fluorescence from the burns relative to adjacent normal tissue were determined from the images and correlated with the depth of burn injury as determined by histology. Six-mm punch biopsies of normal and selected burn sites were taken prior to ICG administration and from normal and all burn sites immediately after recording each image. All biopsies were immediately placed on dry ice. A total of 5 pigs were used for this study.

The frozen tissue biopsy specimen was cut in half, 25  $\mu\text{m}$  sections were cut from one half and used for fluorescence microscopy. Fluorescence microscopy was performed by collaborators at Sandia National Laboratories. Fluorescence micrographs were recorded with a 14 bit, thermoelectrically cooled, electronically shuttered CCD camera (CH230, Photometrics Inc., Tucson AZ) coupled to a microscope (IC5, Olympus, Melville, NY) with a 5X objective (NEO SPlan 5NIC, N.A.=0.13). The output from a 300 mW, 803-nm diode laser (SDL-2351-P2, SDL Inc., San Jose, CA) was coupled to a 0.4 mm core optical fiber and used to illuminate the tissue sample. The output of the fiberoptic was collimated with a 10x objective (M-10X, Newport Corp., Irvine, CA) and passed through two 10-nm bandpass filters centered at 801 nm (54000, Oriel Instruments, Stratford, CT). ICG fluorescence was collected through two 850 nm longpass filters (51360 and 58861, Oriel Instruments, Stratford, CT) selected to effectively reject the light from the illumination source. Image acquisition times were typically 5 s with typical irradiances of 90 mW/cm<sup>2</sup>. The distribution of ICG was determined from the fluorescence micrographs and correlated with the depth of burn injury.

The depth of burn injury was assessed using the second half of the biopsy sample by histochemically staining for lactate dehydrogenase (LDH) activity [Balogh, 1961]. The frozen punch biopsies were incubated in Michaelis' barbital-Na acetate buffer with nitro-blue tetrazolium (Nitro-BT), beta-nicotinamide adenine dinucleotide and sodium lactate. The biopsies were refrigerated in this medium overnight, then rinsed in plain barbital buffer and fixed in 10% formalin. Eight  $\mu\text{m}$  thick sections were then cut and lightly counterstained with eosin. Burn depth was assessed from the slides by measuring the thickness of tissue not stained by nitro blue diformazan. Burn depth, determined from the absence of LDH staining, is plotted as a function of burn duration for 1 hr and 48 hr old burns in Figure 5. The burn depths are greater 48 hours after burn placement for burns of equivalent brass block application times, presumably due to the death of initially viable cells over the 48 hour period. The depth of the burns ranged from superficial to deep dermal. The increase in burn depth with brass block application time follows the expected square root of time dependence ( $\sqrt{kt}$ ) as denoted by the curves through the data, where  $t$  is the burn duration in seconds and  $k$  is related to the thermal diffusivity rate [Henriques, 1947]. The rates were determined to be 0.12 and 0.20 mm<sup>2</sup>/s, for 1 hr and 48 hr old burns respectively.

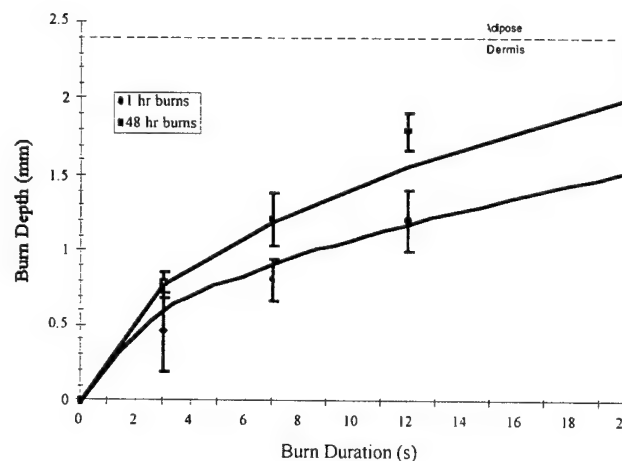


Figure 5. Burn depth as determined by LDH staining versus brass block application time.

The distribution of ICG in normal porcine skin, and 3, 7, and 12 s burns created one hour prior to injection are shown in Figure 6. In general, the fluorescence micrographs of normal skin show a lack of fluorescence in the epidermis and homogeneous low levels of fluorescence in the dermis. The papillary plexus of normal skin occasionally showed a higher level of ICG fluorescence as seen in the figure, although this was not observed in most normal skin specimens. In general, the fluorescence microscopy images of burn sites show three different dermal tissue zones. The intensity of ICG fluorescence in the uppermost layer is essentially negligible. The middle layer shows increased fluorescence and the fluorescence intensity of the lower tissue

layer is reduced and similar to the fluorescence intensity observed in normal tissue. The depth of the enhanced fluorescence band increases with burn application time. For 24 and 48 hour burns, a similar three layer pattern is observed with the exception that the intensity of the middle layer is reduced. Figure 7 shows column-averaged intensity plots for two 7 s burns created 1 and 48 hours prior to imaging and taken from the same animal. The column-averaged intensity profiles for older burns are similar to newly placed burns with the exception that the intensity of the middle layer is reduced. Figure 7 shows a four-fold decrease.

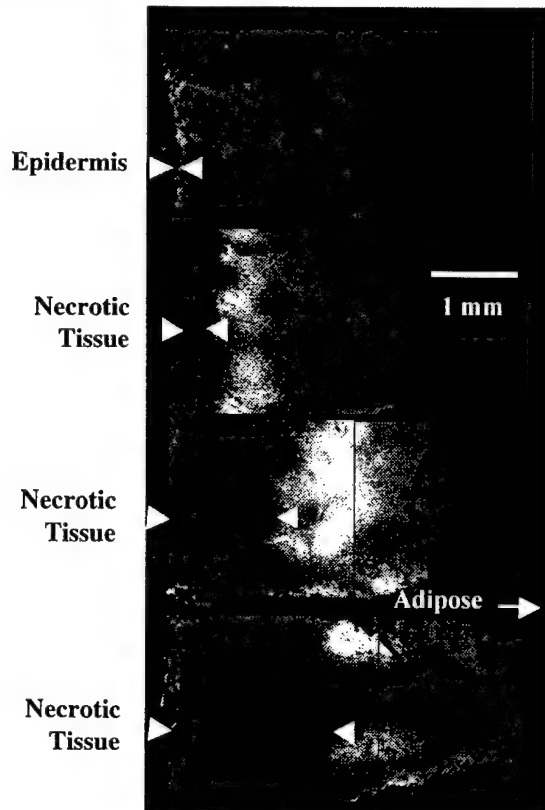


Figure 6. The distribution of ICG determined by the fluorescence from normal and burn tissue. The burns were created one hour prior to imaging. The images (top to bottom) correspond to normal skin and 3, 7, and 12 s burns, respectively. The 7 and 12 s burns are composites of two fields.

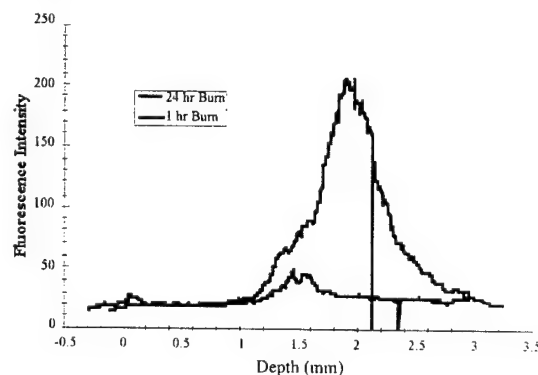


Figure 7. Column-averaged line profiles of the fluorescence intensity of ICG in frozen sections from 7s burns created 1 and 24 hr prior to ICG administration. The sharp negative spikes correspond to where two fields were pieced together.

The uppermost border of the fluorescence band correlates with the boundary separating viable and nonviable tissue as determined by LDH stained slides. Figure 8 plots the burn depth determined by fluorescence micrographs against the value found using LDH staining. The thickness of the dark upper tissue layer correlates

linearly with the depth of burn injury determined from LDH staining. The slope of the line is approximately unity ( $m=0.94$ ) denoting a one-to-one correlation with burn depth. The intercept equals  $48\text{ }\mu\text{m}$ , the approximate thickness of the epidermis ( $60 \pm 24\text{ }\mu\text{m}$ ).

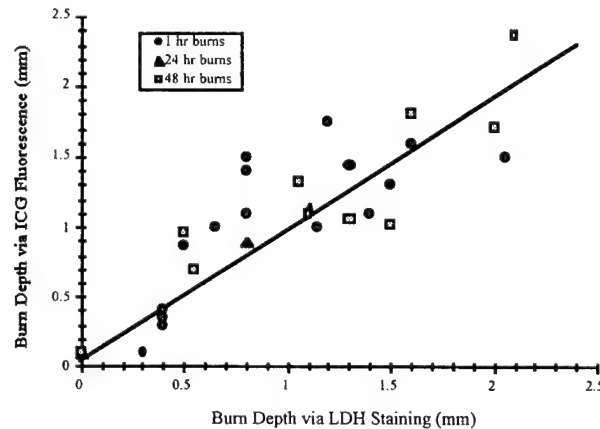


Figure 8. Correlation of depth of burn determined by the onset of ICG fluorescence and LDH staining. The result of a linear regression analysis is represented by a solid line.

The ICG fluorescence images of typical burn wounds are shown in Figure 9. The photo is split into 4 rows, the color photos of 1 hr and 24 hr burn wounds are shown in rows 1 and 2, respectively. The corresponding fluorescence images are given in rows 3 and 4. The three columns correspond to 3, 7 and 12 s burn durations. In general, the amount of fluorescence seen in the wounds decreases with burn duration and also with the age of the burn.

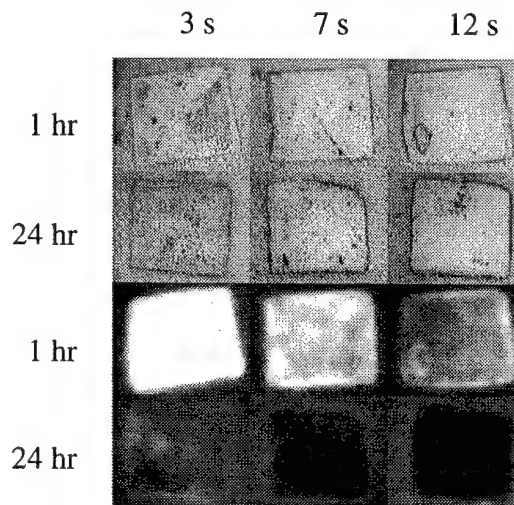


Figure 9. Color and fluorescence images of ICG in burn injured tissue. The color images of 3, 7, and 12 s burns created 1 hr (top row) and 24 hours (second row) and fluorescence images (bottoms 2 rows) are shown.

The ratio of fluorescence measured from the burn wound relative to normal surrounding tissue is plotted in Figure 10. In general, the fluorescence ratio for 24 and 48 hr old burns is less than 1 hr old burns, and decreases exponentially with burn depth. Diffusion theory would predict an exponential falloff in the

fluorescence signal observed at the tissue surface as the signal from this narrow band of fluorescence is shifted deeper into the tissue,  $I_f^0(z) = A_0 \exp(-\mu z)$ . The parameters of the single exponential fit are given in Table 1.

The distribution of ICG in burns is being used to assess burn depth and the need for early surgical excision. Previously, ICG fluorescence was used to assess burns in rat skin where it was found that partial-thickness burns had higher levels of fluorescence compared to full-thickness burns [Green, 1992a]. In general, partial thickness burns have a larger fluorescence signal compared to normal skin while full-thickness burns have a smaller fluorescence signal. This observation was confirmed in humans [Sheridan, 1995]. The larger signal is thought to be due to vasodilation and hyperemia and the smaller signal due to vascular occlusion and edema. This paper supports these hypotheses and presents evidence that vascular permeability also plays a role in enhancing the signal relative to normal tissue.

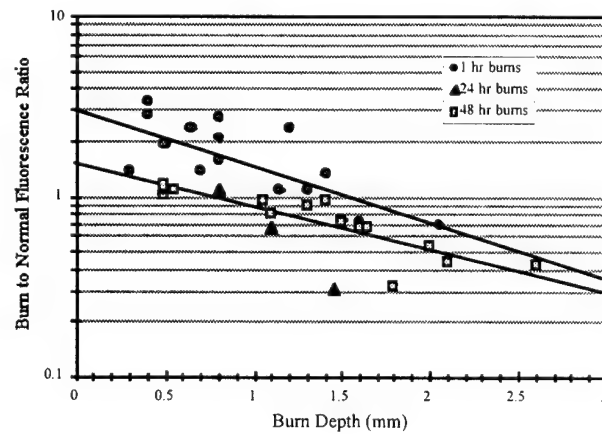


Figure 10. The ICG fluorescence intensity ratio of burns relative to adjacent normal tissue is plotted versus the depth of burn determined by LDH stained slides. The fluorescence intensities were measured at the surface 15 min after administering ICG for burns placed 1, 24 and 48 hr prior to imaging.

Table 1. Fitting parameters to the burn to normal fluorescence ratio data. The data are fitted with a single exponential decay.

Age of Burn (hr)	$\mu$ ( $\text{mm}^{-1}$ )	$A_0$
1	0.70	3.3
48	0.48	1.4

The near-IR absorption of dilute ICG in plasma is bimodal, having a maximum at 805 nm and a minor shoulder at 730 nm [Landsmann, 1976]. The intensity of the 730 nm absorption band is concentration dependent and is attributed to aggregates of the molecule. The emission of ICG in plasma has a maximum at 830 nm [Benson, 1978]. These near-IR wavelengths are ideal for probing tissue as these wavelengths permit relatively deep optical penetration. Thirty-seven percent of the excitation energy measured at the tissue surface reaches a depth of 1.2 mm in fair Caucasian skin [Anderson, 1982], a depth that is generally greater than the boundary separating burns that heal quickly with minimal scarring and deeper burns that will not. In contrast, the optimum excitation wavelength of fluorescein isothiocyanate (FITC) is 500 nm and has a comparable 1/e-penetration depth of 0.25 mm. As a result, fluorescein fluorescence has been shown to be useful in distinguishing superficial partial thickness burns from full-thickness burns but fails to distinguish deep partial-thickness from full-thickness burns [Black, 1986].

Another advantageous property of ICG is that it binds strongly to plasma globulins and in particular to  $\alpha_1$ -lipoproteins (MW 200kDa) [Baker, 1966] limiting both extravasation within burn-injured vascular epithelia

and extravascular transport to areas nearby. ICG is absent from the epidermis of normal skin. Generally, ICG fluorescence was not observed in the epidermis because of the lack of blood vessels, and the diffusion of globulin-bound dye to the epidermis is small. Furthermore, the plot of burn depth determined by ICG fluorescence compared to LDH staining (Figure 8) yields a linear correlation with an intercept of 48  $\mu\text{m}$ . The nonzero intercept is consistent with the lack of fluorescence in the uppermost 48  $\mu\text{m}$  of normal tissue. The mean thickness of normal porcine epidermis was found to be  $60 \pm 24 \mu\text{m}$ .

In this study, a band of increased fluorescence relative to normal tissue was observed lying between the classic coagulated and normal tissue zones [Jackson, 1953] and coincides with the boundary separating viable from thermally inactivated cells as determined from tissue sections stained for lactate dehydrogenase activity (Figure 6). The band of fluorescence was predominantly seen in newly placed burns and the magnitude of fluorescence in this band decreases with burn age (Figure 7). The intensity of the band is dependent on the degree of hyperemia which itself depends on the age of the burn. However, enhanced vascular permeability within this hyperemic zone is also playing a role as the diffuse homogeneous fluorescence pattern seen in the band of fluorescence is consistent with extravasated dye and not dye that is confined to the vasculature. In addition, fluorescence from this band persists relative to normal tissue, suggesting an increased clearance time for ICG in burns due to a greater amount of the drug in the interstitial compartment. The microscopic images were recorded from tissue specimens frozen 15 minutes after administering ICG where the dye is essentially absent from normal tissue (vascular compartment). The increasing burn to normal fluorescence ratios for superficial and deep burns with time following ICG administration is attributed to a longer clearance rate of ICG in burns [Sheridan, 1995].

The origin of this band is believed to be the result of increased vascular permeability of vessels located in the hyperemic tissue zone and *not* the result of increased vascular perfusion of this zone. Laser Doppler flowmetry, used in a recent study for the early assessment of burns [Atiles, 1995], measured a two- and three-fold increase in vascular perfusion for superficial burns on day 2 and 3, respectively compared to measurements made within 12 hr post burn on the same burns. In contrast, we found that the fluorescence intensity of ICG decreases two-fold for comparable superficial burns (see Table 2). The ratio of the exponential prefactors ( $A_0$ ) for 1 hr old burns and 48 hr old burns is 2.4 implying a 5-fold increase in vascular permeability for the 1 hr old burns, if hyperemic effects are neglected.

Although thermally induced vasodilatation (hyperemia) could also account for an increase in ICG fluorescence, the vascular response is complex as vasodilation also leads to increased vascular permeability and edema [Moritz, 1947]. The enhanced filtration rate of ICG in burns is more characteristic of a change in permeability as the pharmacokinetic behavior of dilated vasculature with tight junctions should closely follow the behavior of normal vasculature. In addition, changes in blood volume alone cannot account for 20-fold increases in ICG fluorescence observed within the band and underlying normal tissue (Figure 7). Two distinct phases of increased endothelial permeability of large macromolecules have been shown to exist in burn injuries [Wilhelm, 1960]. The first phase occurs instantaneously with the injury, is mediated by histamines and/or serotonin, is confined to the periphery of the burn, and subsides within an hour. The second phase occurs 1 to 8 hr later, is mediated by other factors, and can last for 2 to 40 hr [Green, 1978]. Furthermore, the dynamics of these microvascular changes depend strongly on the severity of the burn. In particular, the magnitude of the first phase decreases with increasing severity while the onset of the second phase shifts to shorter times. Our observations are consistent with severe burns having a shortened second phase. In the porcine burn model, enhanced vascular permeability was observed in burns created 1 and 2 hr prior to measurement that substantially subsided after 24 and 48 hr. In a similar fashion, the papillary plexus of normal skin occasionally shows a higher level of ICG fluorescence as seen in Figure 6. This enhanced fluorescence might be explained by transient vascular permeability of the skin as the result of clipping during skin preparation.

The intensity of ICG fluorescence in the uppermost necrotic burn layer (eschar) is negligible as the occluded vasculature hinders systemic delivery of ICG to this area. The thickness of this layer is dependent on the application time of the brass block. The change in thickness with burn application time and the lack of ICG in the burn eschar readily explain the decrease in the ICG fluorescence signal recorded from 24 hr old burns as the brass block application time increases (Figure 9). This is expected as the eschar attenuates the amount of excitation light that reaches the underlying tissue where ICG is present, and then further attenuates the fluorescence from these layers as the light returns to the surface. Photon diffusion theory predicts an

exponential decline in the fluorescence signal observed at the tissue surface as a narrow band of fluorescence is shifted deeper into the tissue. A similar exponential attenuation was observed in 1 hr old burns, however the magnitude of the signal (Table 1) is enhanced 2.4 fold due to an increased vascular permeability that subsides over a few hours. The larger exponential decay constant,  $\mu$ , comparing 1 hr and 48 hr old burns in Table 1 may be due to a difference in the optical properties of the burns. However, the picture is somewhat complicated as the magnitude of the inflammatory (permeability) process,  $A(z)$ , is dependent on the severity (depth) of the burn [Wilhelm, 1960], i.e.,  $I_r^0(z) = A(z) \exp(-\mu z)$ .

Burn diagnosis is dichotomous; asking whether the wound will heal or not in 21 days. Determining the depth of a burn from the burn to normal ICG fluorescence ratio is not as clinically relevant as estimating the healing time, however it is a necessary first step to show a dependence on depth. The more important evaluation of predicting which burns will heal with minimal granulation is underway and early results are promising. The latter study was designed to look at different body locations where the relative blood flow and skin thickness are different. Although highly perfused or hypoperfused tissues will exhibit different levels of ICG fluorescence, it is expected that blood flow will have less of an effect on the fluorescence ratio.

In summary, the intensity of ICG fluorescence measured at the surface of the wound for burns of similar age was shown to decrease exponentially with the depth of the burn. The intensity of fluorescence measured at the surface is attenuated by and dependent on the thickness of the coagulated burn eschar. The intensity of fluorescence is also dependent on the amount of extravasated ICG, which is dependent on the degree of vascular permeability and perfusion which varies with the age and severity of the burn. Newly placed, superficial burns have significantly more fluorescence than adjacent normal tissue shortly after burn injury suggesting a strong hyperemic reaction in the superficial dermis with increased vascular permeability and minimal vascular occlusion. The increased signal arises from a zone of hyperemic vasculature with an increased filtration coefficient that allows passage of plasma-protein bound ICG into the extravascular space. For deeper burns, the extravasated protein-bound ICG lies underneath the coagulated tissue zone of the burn, where the occluded vasculature excludes ICG. The increased permeability explains the enhanced fluorescence of partial thickness burns and vascular occlusion the decreased signal associated with deeper injuries and suggests that it is possible to diagnose burns that heal on their own from those that will not by measuring the intensity of ICG fluorescence.

## 5. *Examine alternate optical schemes for improving depth definition*

### Burn Depth Determination

Near-field speckle analysis appears to show promise as an alternative optical method for enhancing the determination of burn depth. Studies using both phantoms and porcine skin burns were performed. The tissue phantom used for this study was composed of a static polytetrafluoroethylene (PTFE) layer and a diffusive intralipid layer. The static layer mimics burn eschar with no blood flow and the thickness of this layer was varied using PTFE sheets ranging in thickness from 0.127 mm to 1.27 mm. The sheets were placed on top of a 7.62 cm diameter glass cylinder filled with a lipid solution (Intralipid-10%, Kabi Pharmacia, Inc.) diluted to 6% to match the scattering properties of the PTFE. The intralipid layer represents viable underlying tissue having blood flow. The scattering coefficient of PTFE was  $23 \pm 4 \text{ mm}^{-1}$  [Sadhvani, 1996] while the scattering coefficient of the 6% Intralipid solution was  $23.2 \pm 0.2 \text{ mm}^{-1}$  [Moes, 1989]. The tissue phantom has negligible absorption. For reference, the scattering coefficient for normal skin at 632.8 nm is  $18.5 \text{ mm}^{-1}$  [Cheong, 1990].

For the porcine skin burns, burns were placed on the backs of anesthetized animals using a 4x4 cm block heated to 100°C by previously immersing in boiling water. To create burns of varying depths, the block was held in place for 1, 3, 5, 7, 12, or 20 seconds. Speckle patterns from burns and normal skin were imaged both 1 hour and 48 hours after placement of the burns. A 4 mm punch biopsy was taken at the same site as the speckle measurement and lactose dehydrogenase (LDH) staining was used to determine the true burn depth at that site [Hukki, 1989]. Staining only occurs if biological activity is present. LDH is easily denatured by heat and its presence is a good assay for viable cells. Three animals were studied.

Figure 11 shows the experimental setup used for this study. The setup consists of a 8 mW helium-neon laser (05-LHP-171, Melles-Griot, Carlsbad, CA), a 30 cm focal length lens used to focus the beam to a

point (beam diameter = 0.2 mm) on the PTFE surface, crossed polarizers, a charged coupled device camera (CCD-C72, MTI-Dage, Michigan City, IN), a frame grabber (Perceptics PixelBuffer, Perceptics Corp., Knoxville, TN), and a Macintosh computer (Quadra 950, Apple Computer Inc., Cupertino City, CA). The crossed polarizers reduce surface speckle and specular reflections. The camera is positioned directly over the speckle pattern while the illuminating laser beam is  $15^\circ$  from normal. This orientation reduces the specular reflectance component which has its highest intensity at  $-15^\circ$  from normal. The resolution of the camera was 11 pixels per millimeter. The acquired image size was 640 pixels by 480 pixels which corresponds to a field of view of 58 mm by 44 mm.

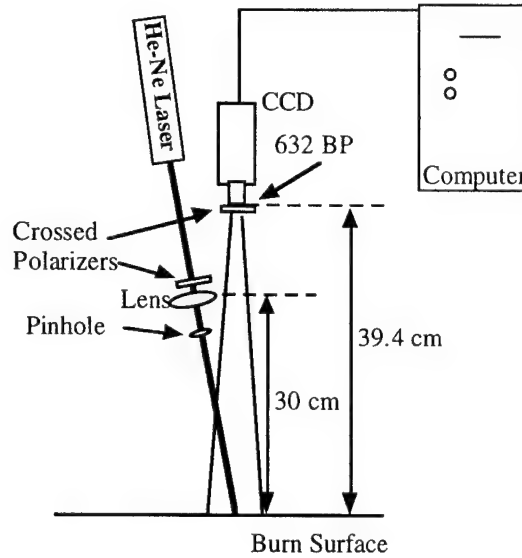


Figure 11. Experimental setup used to acquire speckle images. A HeNe laser is used as the source. The laser beam is focused onto the object by the 30 cm focal length lens. The bandpass filter is used to reduce the effect of room light.

Speckle contrast was determined as a function of radius from the point of irradiation by using an image processing algorithm that determines the mean intensity and standard deviation of the pixels that make up an annulus drawn about the illumination spot. The speckle contrast,  $C(r)$ , is found by:

$$C(r) = \frac{\sqrt{\sigma^2(r) - \sigma_\infty^2}}{\mu(r)} \quad (4)$$

where  $\sigma^2(r)$  is the standard deviation measured at radius  $r$ ,  $\sigma_\infty^2$  is the standard deviation at a radius of 10 mm where it is assumed there is no speckle, and  $\mu(r)$  is the mean intensity of the annulus at radius  $r$ . Before the speckle image is analyzed, a background image (one that is acquired with the illuminating source turned off) is subtracted from the speckle image. This is done to account for the pedestal voltage of the CCD camera. However, the subtraction also introduces additional shot noise which is accounted for by the subtraction of  $\sigma_\infty^2$  from  $\sigma^2(r)$  in equation (4) ( $\sigma_\infty^2 = \sqrt{2}\sigma_{BKG}^2$ ). Neutral density filters (NDF) were placed in front of the camera in order to extract contrast information at smaller diameters where the unattenuated beam can saturate the camera. NDF's having optical densities 0.3, 1.0, and 1.3 were used to give attenuations of 50%, 90%, and 95% respectively. Prior to acquiring a speckle image the first polarizer was adjusted to be parallel to the polarization of the laser. The second polarizer was adjusted to minimize specular reflection from a metal target. The camera is then focused onto the PTFE surface. The aperture of the camera (Nikkor 50 mm f/1.8 AF, Nikon Inc., Melville, NY) was set to f/22, to maximize the speckle lobe size making sure an average speckle lobe is larger than a single pixel ( $1.22\lambda x/d = 134\mu\text{m}$ ). Five speckle images were then acquired for each PTFE sheet with the PTFE sheet being shifted several millimeters between acquisitions. Once all PTFE sheets are imaged, the laser was turned off and a background image acquired.



The radial speckle contrast values for the six PTFE sheets are shown in Figure 12a. The speckle contrast values were determined from the average of five locations on each PTFE sheet, and monotonically decrease with increasing radial distances. Figure 12b shows speckle contrast as a function of PTFE thickness at several different radii. At larger radii, there is little sensitivity to thin sheets. On the other hand, sensitivity to thicker PTFE decreases at smaller radii. The greatest sensitivity to PTFE thickness over the complete range studied occurred at a radius of 0.85 mm. The speckle contrast calibration plot for determining PTFE thickness at a radius of 0.85 mm is shown in Figure 13. The 95% prediction and confidence limits are also shown. The accuracy of this technique for determining PTFE thickness is found to be  $\pm 200 \mu\text{m}$ .

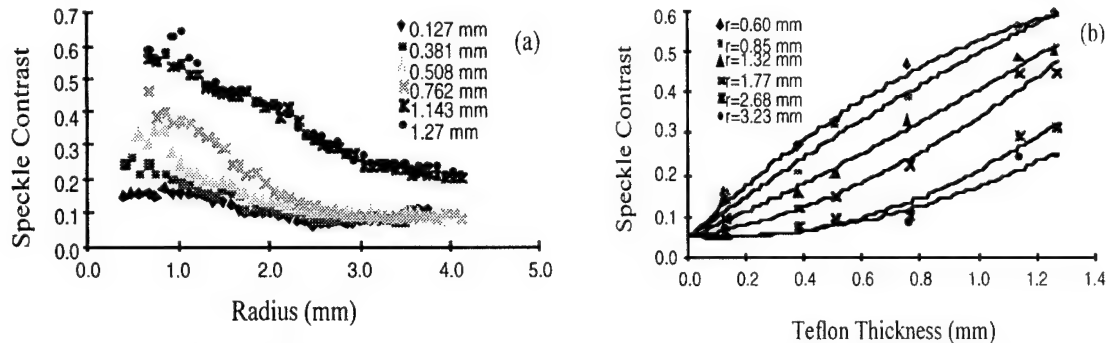


Figure 12. (a) Near field speckle contrast versus radius from the point of irradiation and (b) speckle contrast as a function of Teflon thickness at several radii. Radii of 0.60, 0.85, 1.32, 1.77, 2.68, and 3.23 mm were used. The radius that offers the greatest sensitivity between all thicknesses is  $r=0.85 \text{ mm}$ . The symbols are measured data and the lines are fits.

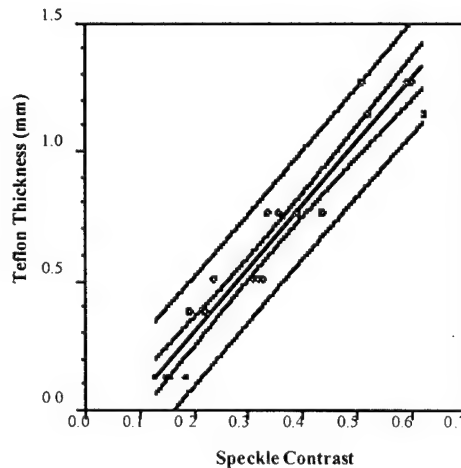


Figure 13. Speckle contrast at a radius of 0.85 mm as a function of Teflon thickness. The central linear line represents a regression analysis fit to the data, having a slope of 2.2 mm. The outer lines represent the 95% prediction intervals. The two inner curves represent 95% confidence limits. The value for the speckle contrast measured at a radius of 0.85 mm can be used to determine the thickness of the Teflon sheet to an accuracy of  $\pm 200 \mu\text{m}$ .

Having a good understanding of how speckle contrast depends on static layer thickness, we moved on to animal experiments. Speckle contrast data from 1, 3, 5, 7, 12, and 20 second burns placed 1 hour and 48 hours previously were measured. Analogous to PTFE, the speckle contrast decreases radially as a larger fraction of photons sample deeper tissue. Figure 14 shows speckle contrast as a function of burn depth evaluated at two different radii, 2.5 and 4.0 mm. Speckle contrast was measured 1 hour and 48 hours after burn placement. A

radius of 4 mm yields the highest sensitivity to burn depths greater than 1 mm. The 95% confidence prediction lines were calculated for burn depths up to 1 and 2 mm for the 2.5 and 4.0 mm radii, respectively. Using a radius of 4.0, the accuracy for determining the depth of 1 hour burns is  $\pm 290 \mu\text{m}$ . For 48 hour burns, the accuracy drops to  $\pm 700 \mu\text{m}$ .

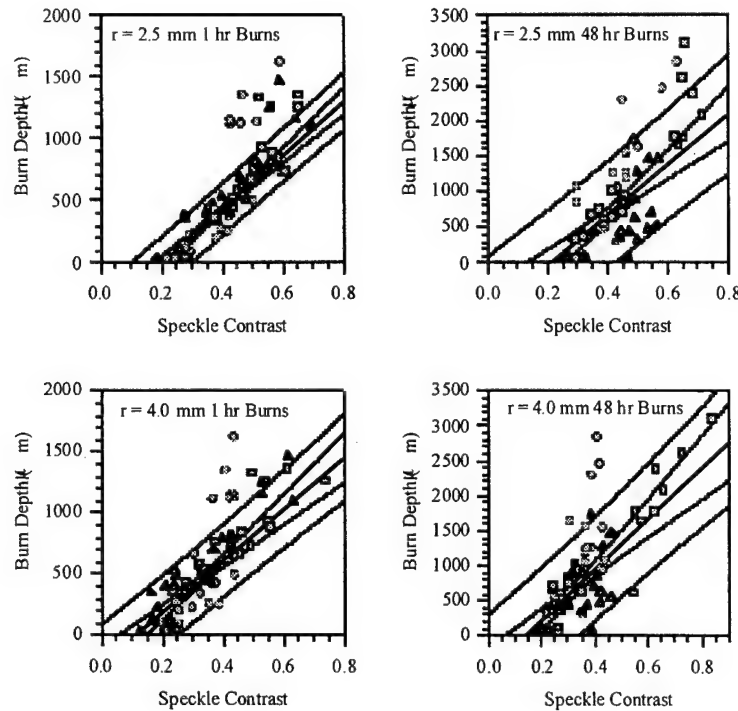


Figure 14. Speckle contrast at a radius of 2.5 and 4 mm as a function of burn depth for burns measured 1 hour and 48 hours after burn placement. The central linear line represents a regression analysis fit to the data. The outer lines represent the 95% prediction intervals. The two inner curves represent 95% confidence limits. Using a radius of 4 mm, the thickness of burns measured 1 hour after placement can be measured with an accuracy of  $\pm 290 \mu\text{m}$ . For 48 hours burns, the accuracy is  $700 \mu\text{m}$ .

If a burn is considered to have a burn eschar layer whose scatterers are stationary overlying a viable tissue layer whose scatterers are in motion (blood flow), then the PTFE/Intralipid tissue phantom can be thought of as a reasonable representation of a burn. Optimization of the processing algorithm using the tissue phantom yielded equation (4) which was used to construct Figure 12 which shows how speckle contrast is dependent on static layer thickness and radius from the point of irradiance. The decrease in contrast with increasing radius was expected because the number of static speckle photons decreases and the relative number of dynamic photons increases. It is the photons that scatter from dynamic particles that modulates the speckle pattern leading to blurring of the integrated speckle image. Speckle contrast information can be determined at radii as small as  $500 \mu\text{m}$  corresponding to 45 pixels sampled. Speckle information at radii smaller than  $500 \mu\text{m}$  could be extracted, however, too few pixels would be sampled to accurately determine the mean and standard deviation.

One method to remove radial dependence is to determine the radius at which speckle contrast has the greatest sensitivity to changing thickness. The speckle contrast values at that radius could then be plotted as a function of thickness. Examining Figure 12, it is apparent that the greatest sensitivity will not be at radii greater than  $2.0 \text{ mm}$  because of the inability to discern between the thinner PTFE thicknesses. Also, the speckle contrast found for smaller radii saturates at 0.6 and must be prevented. Saturation serves to decrease the sensitivity. Therefore, the radius chosen must lie between these two limits. Figure 12 shows that over the

range of PTFE thicknesses analyzed, the best sensitivity of speckle contrast to changing PTFE thickness occurred at a radius of 0.85 mm. Depending on the range of thicknesses under investigation, a different radius could be chosen. For example, if the static layer thickness range is known to be 0.0 mm to 0.50 mm, then the speckle contrast at a radius of 0.60 mm should be used to determine the actual thickness. This is because the speckle contrast at this radius is more sensitive to changing thickness in this range than the speckle contrast at larger radii. Similarly, if it is known that the static layer is > 1.0 mm, then the speckle contrast at a radius of 2.68 mm could be used to determine the thickness. The speckle contrast at this radius can be used to determine the thickness of the static layer to an accuracy of  $\pm 200 \mu\text{m}$  (Figure 13).

When speckle contrast was measured using the porcine skin burn model, the results were similar to the phantom experiment. The dependence of radius on speckle contrast is very similar to Figure 12a. The burn eschar plays the analogous role as PTFE by reinforcing the photon's paths resulting in speckle contrast on the surface. Again, it is necessary to eliminate the dependence on radius in order for speckle contrast to determine burn depth. Figure 14 shows the speckle contrast as a function of burn depth at two different radii measured 1 hour and 48 hours after burn placement. Depending on which radius is chosen, very different results are seen. It seems as though the speckle contrast as measured at a radius of 4.0 mm is most sensitive to changing burn depth, over the range of interest. Using the confidence prediction intervals, the depth of a burn could be determined with an accuracy of  $\pm 290 \mu\text{m}$  by the use of laser speckle contrast at 1 hour after burn placement. Speckle contrast saturates to a value of 0.6 for burns > 1000  $\mu\text{m}$ . Burns measured 48 hours after burn placement, Fig. 8b, have much poorer accuracies. Burn depths can be determined at 48 hours after burn injury with accuracies of  $\pm 700 \mu\text{m}$  at a radius of 4 mm. The poorer accuracies are most likely due to a decrease in the transient hyperemic response leading to reduced blood flow in tissue. It seems that there is nothing gained by waiting 48 hours to diagnose burn depth. It also is more advantageous to the patient to have the depth of the burn determined as soon as possible. Therefore, burns of the same depth imaged both 1 hour and 48 hours after burn placement will not yield the same speckle contrast. It is not clear as to the extent of the effect perfusion has on burns of different depths. Although not shown, the speckle contrast increases with increasing absorption. However, the relative enhancement of speckle contrast with blood absorption is smaller than the change observed by increasing PTFE thickness or burn depth. For example, the change in speckle contrast for PTFE is 0.6 for a thickness range of 0.0 to 1.3 mm. In contrast, the maximum increase in speckle contrast is 0.1 for the 1.143 mm PTFE sheet when  $\mu_a$  was increased from 0.01 to 0.1  $\text{mm}^{-1}$ , the physiological range found in burns. This translates to a maximum error of  $\pm 100 \mu\text{m}$  in assessing PTFE thickness.

#### Optical Properties of Porcine Skin Burns

The optical properties of burned tissue were measured and correlated to speckle contrast. Two techniques were used for determining the absorption coefficient,  $\mu_a$ , and the reduced scattering coefficient,  $\mu_s'$ , of the sample in this study. The first approach determines the optical properties from the radially dependent diffuse reflectance profiles and can be used on tissue *in vivo* or *in vitro*. An equation that describes the radially dependent diffuse reflectance has been devised previously [Farrell, 1992]. For the present analysis, the mean speckle intensity determined from an annulus of radius  $\rho$  centered around the incident beam is equivalent to the diffuse reflectance at that same radius,  $R(\rho)$ . The radially dependent diffuse reflectance for a single scatter source is given by

$$R(\rho) = \frac{a'}{4\pi} \left[ \frac{1}{\mu_t'} \left( \mu_{\text{eff}} + \frac{1}{r_1} \right) \frac{e^{-\mu_{\text{eff}} r_1}}{r_1^2} + \left( \frac{1}{\mu_t'} + 2z_b \right) \left( \mu_{\text{eff}} + \frac{1}{r_2} \right) \frac{e^{-\mu_{\text{eff}} r_2}}{r_2^2} \right], \quad (5)$$

where  $z_0$  is the photon source depth,  $\mu_{\text{eff}} = [3\mu_a(\mu_a + \mu_s')]^{1/2}$  is the effective attenuation coefficient where  $\mu_s' = (1-g)\mu_s$  with  $g$  being the average cosine of the forward scattering angle,

$$r_1 = [(z - z_0)^2 + \rho^2]^{1/2}, \quad (6)$$

and

$$r_2 = [(z + z_0 + 2z_b)^2 + \rho^2]^{1/2}. \quad (7)$$

The parameter,  $z_b = 2AD$ , defines the location of this negative image point and is dependent on the index mismatch of the boundary, where

$$D = \{3[\mu_a + (1-g)\mu_s]\}^{-1} \quad (8)$$

is known as the diffusion constant. If the indices of refraction were equal on each side of the boundary,  $A$  would equal 1. For PTFE,  $A$  equals 3.6. The transport albedo and total interaction coefficient are given by  $a' = \mu_s'/\mu_t'$  and  $\mu_t' = \mu_a + \mu_s'$ , respectively. Equation (5) is the closed form solution for predicting the reflectance at the object's surface. Except for the parameters  $\mu_a$  and  $\mu_s'$ , all other parameters in equation (5) are known. It has been shown that the results using equation (5) closely match data produced through the use of Monte Carlo modeling [Farrell, 1992]. The equation is strictly valid for homogeneous one layer samples. The second technique used to determine the optical properties of the irradiated sample *in vitro* is to determine the percent total diffuse transmission, %T, and the percent total diffuse reflectance, %R. This was accomplished through the use of a double beam, double monochromator spectrophotometer adapted with a 15 cm diameter integrating sphere (UV 5270, Beckman Instruments, Fullerton, CA). An inverse-adding-doubling (IAD) routine was performed using the measured values of %T and %R to yield  $\mu_a$  and  $\mu_s'$  [Prah, 1993].

Slabs of burned and normal porcine skin were excised in order to measure %T and %R to determine the optical properties. The burns were of durations 3, 7, and 20 seconds and were excised 48 hours after burn placement. The preparation of the skin slabs was quite straight forward. Care was taken to remove most of the fat from the sample to leave only dermis and epidermis. The sample was first imaged using the setup shown in Figure 3 and then sectioned. Each section was mounted between two glass slides and the %T and %R were measured. Percent diffuse transmission, percent diffuse reflectance, and sample thickness are required to determine the optical properties of the specimen. The samples were kept moist with a saline solution throughout the experiment. Punch biopsies were taken and actual burn depth was determined via LDH staining.

Absorption was added to the PTFE burn model through the addition of human blood to the Intralipid layer to learn how absorption effects speckle contrast. Different concentrations were achieved through dilutions which resulted in five absorptions with corresponding  $\mu_a$ 's of 0.15 mm<sup>-1</sup>, 0.062 mm<sup>-1</sup>, 0.033 mm<sup>-1</sup>, 0.0087 mm<sup>-1</sup>, and 0.0025 mm<sup>-1</sup>. These concentrations were chosen to cover the range of absorptions being measured with burned porcine tissue *in vivo*. Two layered photon migration theory was used to model the behavior of  $\mu_a$  versus PTFE thickness. This is because the absorber is only found in the Intralipid layer and not in the PTFE layer. The equation for  $\mu_a$  determined from a fractional percentage of the  $\mu_a$ 's from the PTFE and Intralipid layers is given as

$$\mu_{a,eff} = \left(1 - \frac{d}{d+z}\right)\mu_{a_0} + \left(\frac{d}{d+z}\right)\mu_{a_{PTFE}} \quad (9)$$

where  $d$  is the PTFE thickness,  $\mu_a$  is the absorption coefficient measured with no PTFE present and is allowed to vary by the fitting routine, and  $\mu_{a,PTFE}$  is the absorption coefficient of PTFE which was found to equal 0.0002 mm<sup>-1</sup>. The parameter  $z$  is the effective probe depth into the Intralipid layer measured from the bottom of the PTFE sheet and is found through the use of:

$$z = \frac{-\ln \alpha - \mu_{s,PTFE}' d}{\mu_{s,Intralipid}' + \mu_{a_0}} \quad (10)$$

where  $\mu_{s,PTFE}'$  is the reduced scattering coefficient for PTFE with a constant value of 5.1 mm<sup>-1</sup>,  $\mu_{s,Intralipid}'$  is the reduced scattering coefficient of Intralipid 6% with a constant value of 6.7 mm<sup>-1</sup>, and  $\alpha$  is defined as the ratio of incident intensity to the intensity at probe depth  $z$  and is allowed to vary by the fitting routine.

The optical properties  $\mu_a$  and  $\mu_s'$  were determined for each speckle contrast measurement site using the measured mean intensity as a function of radius from the point of irradiance and Eq. 5. Figure 15a shows the measured  $\mu_a$  as a function of PTFE thickness with data fit lines determined using the diffuse reflectance theory. For thin PTFE sheets, the effective  $\mu_a$  approaches the known  $\mu_a$  of the Intralipid layer. For thicker PTFE sheets, the effective  $\mu_a$  is reduced as less photons probe the Intralipid layer. Figure 15b shows the measured  $\mu_s'$  as a function of PTFE thickness for the five known absorption values. The known values for  $\mu_s'$  of Intralipid 6% and PTFE are also shown on the plot as a solid and dotted line respectively. For thin sheets,  $\mu_s'$

approximates the scattering coefficient of Intralipid. For thicker sheets,  $\mu_s'$  approximates the scattering coefficient of PTFE.

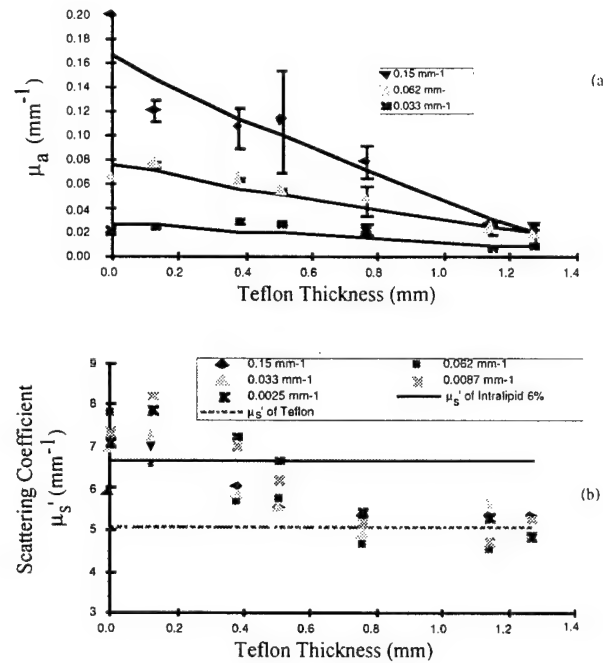


Figure 15. Measured (a)  $\mu_a$  and (b)  $\mu_s'$  via diffuse reflectance versus Teflon thickness. The lines in (a) represent fits to the data assuming the effective  $\mu_a$  is the sum of the respective fractional percents from the two layers (Eq. 3). In (b), the solid line represents the known  $\mu_s'$  of Intralipid 6% and the dashed line represents the known  $\mu_s'$  of Teflon.

The optical properties  $\mu_a$  and  $\mu_s'$  were also determined for porcine skin burns using the speckle contrast measurement site by using the mean intensity as a function of radius from the point of irradiance and Eq. 9. Figure 16 shows  $\mu_a$  and  $\mu_s'$  versus burn depth *in vivo* for sites measured 1 hour and 48 hours after burn placement. Normal and burned porcine skin samples had their optical properties determined *in vitro* both by measuring the mean speckle intensity as a function of radius from the point of irradiance and fitting it with Eq. 9 and through the use of the Beckman spectrophotometer. The results are shown in Figure 17 and generally show good agreement between the two techniques.

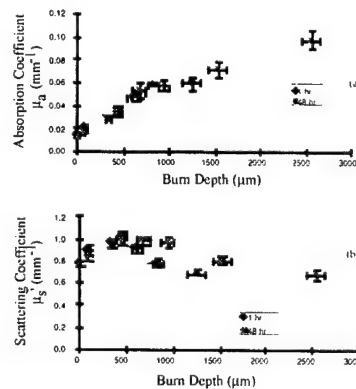


Figure 16. Optical properties measured 1 hour and 48 hours after burn placement *in vivo* using the radial dependent mean speckle intensity data and Eq. (2) versus burn depth. The absorption coefficient is shown in (a) and the reduced scattering coefficient is shown in (b). Each series contains six points corresponding to the mean burn depth average for each of the six burn durations.

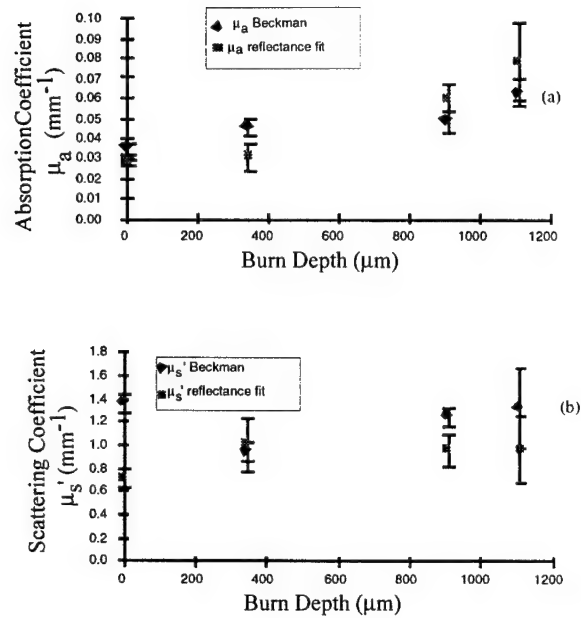


Figure 17. Optical properties, (a)  $\mu_a$  and (b)  $\mu_s'$ , of burned and normal porcine skin in vitro as a function of burn depth.

In summary, the optical properties of the tissue phantom and porcine skin burns were determined. The fitting technique used to determine the optical properties is based on the diffuse reflectance equation developed by Farrell, et al. and is only intended to be used with single layered models. It was necessary to determine the effects of having a two layered model on the fitting routine to better understand the optical properties being determined of the porcine skin burn model *in vivo*. Figure 16a,b shows both  $\mu_a$  and  $\mu_s'$  are dependent on burn depth. As the depth of burns increase, so too does  $\mu_a$ . By eye, one would predict that increasing burn depth would yield a lower value of  $\mu_a$  because of the appearance of the eschar becomes more white and waxy. Upon further thought, the form of Figure 16a is not surprising. It seems that the amount of perfusion changes with burn depth and since blood is the primary absorber of the probing light, absorption should change as well. In fact, the three-fold increase in absorption over the range of burn depths is quite remarkable. The change in perfusion may also explain the form of Figure 16b. With increased perfusion, vascular infiltrate increases serving to increase the density of scatterers which results in an increased  $\mu_s'$ . As the burn depth increases, the vascular infiltrate gets pushed down, thus having less of an effect on the probe volume. This may explain why  $\mu_s'$  falls off with burns > 500 μm. Since perfusion is greater for the same burn depth in 48 hour burns than 1 hour burns, it stands to reason that the vascular infiltrate will be larger in 48 hour burns resulting in a higher scattering density. This may explain the difference in fall off rate between the 48 hour data and the 1 hour data in Figure 16b.

## II. Laser Debridement System

### 1. Formulate design criteria for a laser debridement system based on our preliminary data and acquire the necessary components

A prototype laser debridement system was designed, constructed and tested in a porcine skin burn model. Technical specifications of this system are given in Appendix B.

### 2. Construct a prototype system for burn debridement

A radio-frequency excited carbon dioxide laser (Coherent, Diamond 64, Palo Alto, CA) was used to debride porcine skin. A schematic of the laser burn debridement system is shown in Figure 18. The radio

frequency was 6 kHz with a 50% duty cycle. The delivered power to the tissue was 145-175 Watts. The beam was focused by a single ZnSe lens with a focal length of 75 cm, giving a beam diameter of 1.4 x 1.6 mm at the target. The irradiance was calculated to be 8.2-9.9 kW/cm<sup>2</sup>. The region of ablation was controlled using a x-y galvanometric scanner (General Scanning, G300 Series Galvanometer Optical Scanner, DE Series Digital Electronics, Waltham, MA) that raster scanned the beam over the tissue surface. The scanning velocity along the x-axis was adjusted to give a radiant exposure of 35 J/cm<sup>2</sup> along its axis. The y-axis was stepped following each line scan. The interline spacing of the along the y-axis was set to 0.7 mm, half the beam diameter.

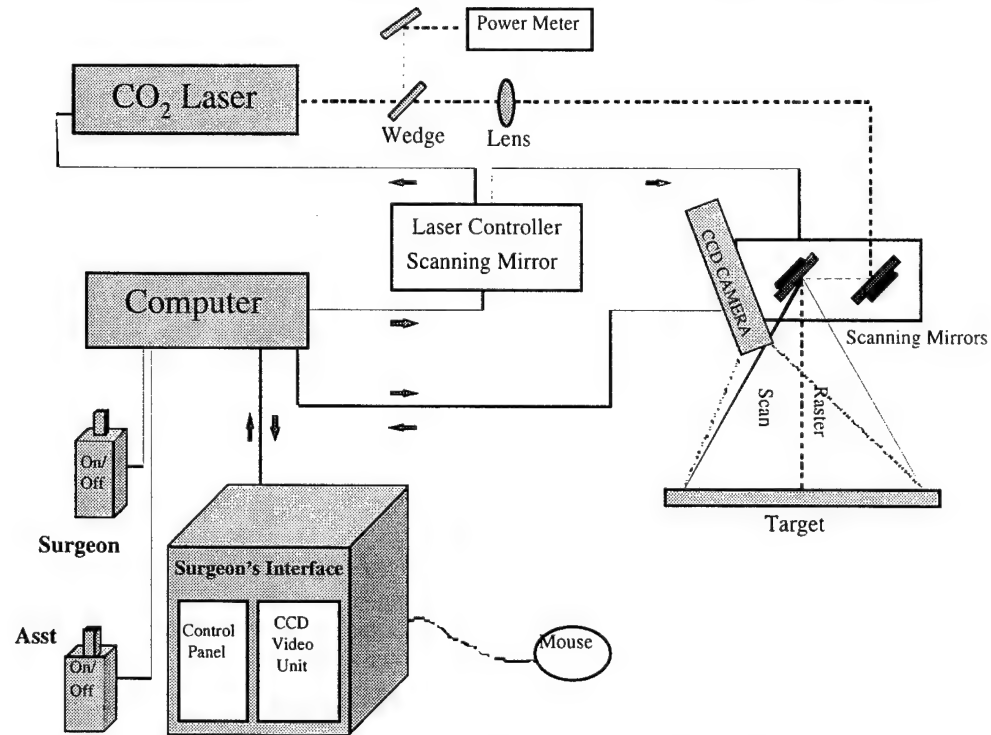


Figure 18. Schematic of laser burn debridement system demonstrating the interrelationships of the laser, computer, and "surgeon's" interface.

A red diode laser was used to adjust the height of the optical deck to focus the carbon dioxide beam onto the tissue surface. The diode laser beam was split into two beams and sent to mirrors on opposite sides of the optical deck. The mirrors were adjusted to superimpose the two red beams with the carbon dioxide beam at the focal plane with the x-y scan mirrors in their plumb position. A frequency doubled, passively Q-switched Nd:YAG laser was adjusted to be colinear with the 10.6  $\mu$ m invisible carbon dioxide beam. Dual series fail-safe switches were used as a safety feature. This allowed the surgeon to disarm the laser should any potential problem arise. Operation of the laser required two persons to activate their respective switches following a designated sequence.

A computer interface is an integral component of the laser system. This enables a surgeon to image a burn area and select a region of debridement. Using a computer pointer, the surgeon can then outline an updated area of debridement after each set of laser passes. In using such an efficient debridement system, a large plume of smoke is produced due to high rates of tissue ablation. This required a high-throughput smoke evacuator (Model 1201-Plumesafe, Buffalo Filter Buffalo, NY) to remove noxious and potentially toxic smoke from the operative field. Along with the smoke evacuator, a specially designed smoke evacuator enclosure was fabricated to confine the large volume of smoke and to actively draw the plume away from the laser beam. Although, a risk of viral transmission from the vaporization plume may exist, we are not aware of any published controlled studies where adverse effects were reported. A high-power smoke evacuation system as the one described above may reduce this risk. The use of appropriate maskwear would further reduce potential exposure to stray viral particles.

### *3. Test and optimize the system in animals*

Although early excision and grafting of deep dermal and full thickness burns has improved patient survival [Tompkins, 1986], shortened hospital stay [Tompkins, 1986] and reduced mortality from burn wound sepsis [Sheridan, 1994], extensive blood loss during burn debridement is a source of ongoing morbidity [Desai, 1990]. The potential for viral transmission [Morris, 1994; Aach, 1991], dilutional thrombocytopenia, intraoperative hypothermia, pulmonary dysfunction [Robinson, 1982], immunosuppression [Waymack, 1991; Graves, 1989], and increased cost [Mann, 1994; Sittig, 1994] due to blood transfusions warrant investigations to reduce such risks. Recently, investigators have explored the role of vasoconstrictive agents [Roberts, 1984; Snelling, 1983; Siegal, 1973; Hartford, 1980] injected into donor and escharotomy sites, the use of topical thrombostatic agents [Stuart, 1988] during debridement as well as the use of tourniquets [Rosenberg, 1986; Marano, 1990] to limit blood loss and oozing from wound beds in extremity burns. While these measures have shown some promise for reducing intraoperative blood loss, the search continues for more efficient methods of limiting blood loss and decreasing the need for transfusions.

The use of continuous wave carbon dioxide lasers as cutting tools to debride burn eschar was first studied in the early 1970's as a means of reducing blood loss [Levine, 1972; Levine, 1975a; Levine, 1975b; Slutzki, 1977]. Reduced bleeding secondary to extensive coagulation at the edge of laser ablated wounds was demonstrated [Levine, 1975a; Levine, 1975b; Slutzki, 1977; Hall, 1971; McKenzie, 1983; Gillis, 1983; Hambley, 1988; Flemming, 1986; Buecker, 1984], but this same tissue damage caused delayed wound healing and prevented successful skin grafting [Fry, 1980; Fidler, 1981; Fidler, 1983; Montgomery, 1983; Buell, 1983; Moreno, 1984; Jarmuske, 1990]. A new approach to this problem is based on the fact that a very brief exposure to a high-energy carbon dioxide laser will result in tissue vaporization with minimal residual thermal damage if the laser exposure time (pulse duration) is less than the heat conduction time (thermal relaxation time) of the tissue [Walsh, 1988; Green, 1992b; Green, 1993; Schomacker, 1990; Domankevitz, 1997; Lucchina, 1994].

The goal of this study was to compare high power continuous wave carbon dioxide laser ablation with surgical excision for the removal of full thickness burns in a porcine burn model. Immediate autografting was performed and graft take was evaluated following tangential laser and surgical excision. Wounds were evaluated clinically and histologically for 180 days to document any long term differences in wound healing between laser and surgically excised sites.

Eleven female Yorkshire farm swine (Parsons, Inc., Hadley, MA) weighing approximately 25 kg were cared for in a manner that conformed to the NIH Guide for Care and Use of Laboratory Animals. The experimental protocol was approved by the Massachusetts General Hospital Institutional Animal Care and Use Committee and the Subcommittee on Research Animal Care. Prior to burn placement, each pig was sedated with ketamine (20 mg/kg IM) and placed left side down on the operating room table. Halothane (0.5-2% to effect), oxygen (4l/min), and nitrous oxide (1-2 l/min), were delivered through a mask. After induction, the rate of halothane administration was decreased to 1 to 1.5% as tolerated. Heart rate and peripheral oxygen saturation were monitored throughout the procedure. The right paravertebral region and torso of the pig were clipped with an electric razor, then washed with chlorhexidine soap and providone-iodine solution.

The burn sites were placed on the right paravertebral region. A 6 cm x 6 cm brass block was preheated in boiling (100°C) water and then held with mild pressure upon the skin surface for 20 seconds to create a full thickness burn. The brass block was reheated between each application. Two burns were placed per pig. The wounds were dressed with silver sulfadiazine cream 1% (Thermazene, Sherwood Medical, St. Louis, MO) and a layer of petrolatum dressing (Xeroform, Sherwood Medical, St. Louis, MO), and covered with sterile gauze. The dressings were fixed in place with an elastic adhesive bandage and stapled to the skin. A garment formed from Stockinette (Alba-Waldensian, Rockwood, TN) was used to protect the wounds from destruction in the animal cage. An intramuscular injection of buprenorphine 0.3 mg (Reckitt and Colman, Hull, England) was given for analgesia upon termination of burn placement, followed by acetaminophen 120 mg every 4-6 hours as needed.

Forty-eight hours after burn placement, the pig was anesthetized again using ketamine, halothane and nitrous oxide as described above. In addition, the animal underwent endotracheal intubation with ventilatory support. It was necessary to intubate the animal prior to laser debridement in order to halt respirations while the laser scanned over the tissue surface. This was facilitated by the use of the neuromuscular blocking agent



pancuronium (Elkins-Sinn, Inc, Cherry Hill, NJ) 0.1 mg/kg IV induction dose with a maintenance dose of 0.015 mg/kg every 25-40 minutes. An 18 gauge catheter was placed in an ear vein for IV infusion of 0.9% NS at 125 cc/hour. One gram of Cefazolin (Marsam Pharmaceuticals, Inc., Cherry Hill, NJ) was administered intravenously 30 minutes prior to laser debridement. The heart rate and peripheral oxygen saturation were monitored via pulse oximetry.

After induction of anesthesia, the burns were exposed and the animal was prepped and draped in a sterile fashion. The site selected for laser debridement was chosen randomly for each animal. The smoke evacuator enclosure was sealed around the laser debridement site and laser scans were delivered in groups of two or four until ten scans had been completed. After ten scans, the adipose tissue was visualized and the liquefied fat was wiped away with sterile gauze. Wiping was repeated between subsequent scans in order to prevent ignition of oil collecting over the tissue surface during ablation. The number of scans performed at each burn site was determined by the appearance of the wound bed. Laser debridement was complete when the erythema, purpura and thrombosed vessels in the burn eschar were removed and moist yellow fat was visualized.

One full thickness burn on each pig was manually debrided to adipose tissue with a hand-held Goulian dermatome (Weck and Co., NY, NY) by an experienced surgeon. This served as the control site. The Goulian Blade removed approximately 1 mm of tissue per tangential cut.

The skin on the right paravertebral region and torso was prepared for split-thickness autograft harvest. The grafts were harvested with a compressed nitrogen gas driven dermatome (Model # 102725, Zimmer, Dover, Ohio) set at 0.016 inches. The harvested skin was placed on a plastic dermacarrier (Model # 2195-12, Zimmer, Dover, Ohio) and expanded at 1:1.5 through a mesher (Zimmer, Dover, Ohio). The grafts were cut to fit the 6 cm x 6 cm debrided burn wounds with minimal expansion of the mesh. Grafts were placed over the laser and surgically debrided burns. Autografts were attached to the skin using 2-0 silk sutures applied every 1 cm around the periphery of the wound. The grafted wounds were then covered with a tie-over stent of petrolatum gauze and sterile dry cotton roll which was anchored tightly by silk sutures.

The donor sites were dressed with Scarlet Red Ointment Dressing (Sherwood Medical, St. Louis, MO.) and layers of sterile gauze which were attached to the wound with 2-0 Nylon suture. The pigs were dressed in 8 inch stockinette with holes cut for the legs. An injection of buprenorphine 0.3 mg IM was given for pain and followed by acetaminophen 120 mg every 4-6 hours as needed. The animal was returned to its cage as the anesthesia began to wear off and was given food and water ad lib.

Burn depth was evaluated by taking a 4 mm punch biopsy of the burn 48 hours after burn placement. Biopsies were evenly divided. One half was fixed in formalin, then processed with hematoxylin and eosin stain. The remaining half was frozen and processed with lactate dehydrogenase (LDH) stain. The LDH stain is a vital dye which stains purple only in viable cells. The lack of staining with LDH denotes cells killed at 47°C [Balogh, 1961] and provides a sensitive and precise measurement of burn depth by immediately revealing the extent of irreversible tissue injury. One half of each biopsy specimen was immediately frozen after excision, incubated in Michaelis Barbitol-Na Acetate Buffer with paranitrophenyl-substituted ditetrazolium salt (Nitro-BT), betanicotinamide adenine dinucleotide and sodium lactate (salt), and then placed in minus 80 degrees Celsius overnight. Subsequently, the tissue was rinsed in plain barbitol buffer, fixed in 10% formalin and processed for routine light microscopy. Before light microscopy, the specimens were dehydrated and stained with a diluted alcohol/eosin solution. This additional step made the unstained tissue (nonviable cells) easier to visualize due to the eosin acting as a counterstain. Burn depth was measured from the LDH-stained specimens using a calibrated reticle under light microscopy instead of H & E stained specimens because of greater sensitivity associated with LDH stain. Tissue measurements were evaluated in at least three random positions in each specimen. Specimens stained with H & E stain were utilized to evaluate histologic graft take and to assess the thickness of granulation tissue (neovascularization, immature and edematous collagen, and a dense cellular infiltrate) between the native subcutis and graft-wound bed interface.

The laser-induced residual thermal damage in the graft bed was measured by taking a 4 mm punch biopsy of the wound immediately after laser ablation of the eschar. One half of each biopsy was processed and stained with hematoxylin and eosin while the remaining half was immediately frozen for LDH stain as described above. The residual thermal damage was measured using the LDH stained slides with a calibrated reticle.

Measurements were made from at least 3 random sites on the tissue specimen. H&E stained specimens were used for comparison of findings noted on LDH stain.

Graft take was evaluated on postoperative day 7 by a blinded examiner. After each dressing was removed, wounds were coded with colored labels. Photographs were taken for comparison and review of wound sites. The examiner rated percent engraftment as defined by revascularization (blanchability) and graft adherence. A paired two sample t-test was used to analyze graft take between laser and manual sites.

Vancouver scar assessments [Sullivan, 1990] were utilized to evaluate long term scarring in five of eleven animals over six months. The Vancouver scar scale is a composite score of four parameters used to evaluate a burn wound. Each parameter has a numerical range to assess severity of scarring. The lower an absolute overall score, the less significant the presence of scarring. Pigmentation, vascularity, pliability and height combine to produce the score. The numerical assignments are as follows: Pigmentation (0=normal, 1=hypopigmentation, 2=hyper-pigmentation) vascularity (0=normal, 1=pink, 2=red, 3=purple), pliability (0=normal, 1=supple, 2=yielding, 3=firm, 4=banding, 5=contracture) and height (0=normal or flat, 1:<2mm, 2:<5mm, 3:>5mm). Cumulative scores range from 0-13. As a result of the similarities between human and porcine skin [Hebda, 1990; Montagna, 1964; Swindle, 1986], it was employed in this study as a method to quantitatively evaluate wound appearance in swine. A surgeon blinded to the mode of excision determined Vancouver scores for wound sites every thirty days. A decision to follow only five of the eleven animals for six months was based on cost as well as study design. The purpose of the first six animals enrolled in the study was to examine engraftment and wound appearance to POD 30. The remaining five animals were primarily used to study long-term scarring over six months.

Punch biopsy specimens (4 mm) were taken from the graft bed on postoperative day 7 and at weekly intervals up to postoperative day 30. Thereafter, biopsies were obtained at monthly intervals for the next five months in the remaining five animals in the study. The biopsies were fixed in formalin, embedded in paraffin, sectioned and stained with hematoxylin and eosin stain for light microscopy. Histologic assessment of graft take was determined by evidence of epidermal viability, neovascularization at the graft-wound bed interface, the presence of a perivascular infiltrate (circulating cells within the graft dermis) and the absence of wound denudation or tissue necrosis. Wound healing was compared between autografts on the laser sites versus manual sites. The width of the zone of granulation tissue at the graft wound bed interface was measured with a calibrated reticle and tabulated for POD 7-180.

### ***Post Operative Day 0***

#### **Burn Depth**

The mean burn depth was measured in ten of eleven animals and found to equal  $2.3 \pm 0.5$  mm. (Table 2). The mean epidermal-dermal thickness was  $2.5 \pm 0.3$  mm. When burn depth is compared to the epidermal-dermal thickness, it is evident that 90% of all the burns placed were in the deep dermis or into adipose. Regardless of the actual burn depth, all of the laser ablated burns were debrided to adipose tissue.

Table 2. Thermal Damage Evaluation of Histologic Specimens: Thermal damage data summarizing burn depth and residual thermal damage. All burns were debrided to adipose regardless of initial burn depth. Three random measurements were taken on each sample after biopsy and microscopic preparation to arrive at mean values. (N/A= data unavailable)

Pig #	Mean Burn Depth ( $\mu$ m)	Epidermal -Dermal Thickness ( $\mu$ m)	Laser Induced Thermal Damage ( $\mu$ m)
1	N/A	2280	N/A
2	2000	2750	200
3	1300	2750	150
4	1950	1950	200
5	2000	2370	100

6	2630	2500	250
7	2880	2700	N/A
8	2700	2440	140
9	2750	2750	190
10	2900	2870	180
11	2500	2620	180
<b>Mean Values +/- S.D.</b>	<b>2360 ± 520</b>	<b>2540 ± 270</b>	<b>180 ± 40</b>

### Residual Thermal Damage

The laser-induced zone of residual thermal damage as measured by the LDH stain (Table 2), was comprised of a thin layer of non-vital cells with a mean thickness of  $0.18 \pm 0.04$  mm on the surface of the adipose tissue of the wound bed. It was difficult to detect the residual thermal damage of the tissue stained with the H & E stain due to the modest amount of collagen distributed in adipose tissue. Thus, LDH results were used to assess this aspect of laser-induced injury.

### Blood Loss

Laser treated sites were nearly bloodless. During the study, one instance of breakthrough bleeding occurred which subsequently resolved after a repeat laser scan. Manually treated sites required tamponade, topical epinephrine and electrocautery to achieve hemostasis. Two standard surgical sponges were usually saturated with blood by the end of the manual procedure.

### Time of Debridement

A similar amount of time was required for laser ablation and manual excision. At a mean power of 153 W, the laser completed one pass in 12.7 sec. Mean lasing time to bloodlessly debride a 6-cm x 6-cm wound site to adipose (13-18 passes) was 3.4-3.8 minutes. Additional time was necessary to set up the laser and to remove oil or debris from the wound bed between laser passes. Between 6-10 passes of the Goulian blade were needed to manually debride the wound to adipose. The approximate time to complete manual debridement was 5-8 minutes, including time to achieve hemostasis which required tamponade and occasional electrocautery.

### ***Post Operative Day 7***

#### Graft Take

On postoperative day 7, the split thickness autografts were evaluated for graft take. Grafts placed on the laser ablated wound bed appeared grossly identical to the manual sites. Although the interstices of the mesh were more prominent in laser ablated sites, both grafts were pink, blanched with pressure, and were firmly adherent to the wound bed. The mean percentage graft take for laser and manual sites were statistically equivalent (Table 2). Among manual sites, the mean percent graft take was  $96 \pm 11\%$ , while in laser ablated wounds, mean graft take was  $93 \pm 8\%$  ( $p > 0.05$ ). On POD 7, laser ablated sites were more vascular and hyperpigmented when compared to manual sites. In contrast, manual sites displayed a shinier appearance and smoother texture on POD 7.

### ***Long Term Wound Healing***

#### Histology

By POD 7, the epidermal interstices were reepithelialized in both the laser and manually debrided sites and the epidermal thickness and architecture appeared normal. A mixed inflammatory infiltrate was present at the graft-wound bed interface. The infiltrate was immediately present at POD 7 in the laser sites, but its magnitude regressed at later times. It took an additional week for the inflammatory cell response to peak in the

manual sites (POD 14). Rare foreign body granulomas were observed in greater numbers in the dermis of laser debrided sites (in response to hair and denatured collagen).

The most apparent difference between the laser and manual sites was the thickness of newly formed granulation tissue between the native subcutis and graft dermis. To quantify this effect, the thickness of granulation tissue was measured in all postoperative sites and tabulated in Table 3. It is evident from Table 3 that the laser debrided sites had a significantly greater amount of granulation tissue at POD 7 than manual sites ( $p < 0.05$ ). However, based on the data, there were no significant differences noted in the thickness of granulation tissue from laser or manual sites from POD 14-180 ( $p > 0.05$ ). The thickness of granulation tissue peaked at POD 60 in both laser and manual sites, and then decreased over the next 120 days.

**Table 3. Overall Data Summary.** Multi-variable data analysis for comparison of laser and manual debridement of full thickness burns.

Variable	N	Laser ( $\pm$ SD)	Goulian Blade ( $\pm$ SD)	p-value
<b>Thermal Damage (<math>\mu</math>m)</b>	11	180 $\pm$ 40	0	N/A
<b>Graft take (%) at POD 7</b>	11	93 $\pm$ 8	96 $\pm$ 11	0.07
<b>Zone of Granulation (<math>\mu</math>m)</b>				
POD 7	11	1010 $\pm$ 710	424 $\pm$ 260	0.01
POD 14	11	1300 $\pm$ 870	740 $\pm$ 530	0.11
POD 21	11	1580 $\pm$ 970	1080 $\pm$ 440	0.12
POD 30	11	1290 $\pm$ 660	1430 $\pm$ 1100	0.81
POD 60	6	1780 $\pm$ 190	1700 $\pm$ 1160	0.83
POD 90	6	1690 $\pm$ 520	1060 $\pm$ 340	0.054
POD 120	6	1300 $\pm$ 880	1430 $\pm$ 910	0.65
POD 150	6	1050 $\pm$ 840	1060 $\pm$ 770	0.97
POD 180	6	1060 $\pm$ 950	720 $\pm$ 500	0.23

### Clinical Assessment

The Vancouver Scar Assessment was followed for wounds in five of eleven animals over a six month period after skin grafting (Figure 19). The most distinct differences observed between the laser and manual sites were related to the degree of pigmentation, vascularity, and pliability of the wound beds. At POD 30, laser debrided wounds appeared to be more vascular and hyperpigmented but less pliable than the manually debrided sites. The height of the overall scar was comparable ( $< 5$ mm) in both groups. The differences were reflected by the Vancouver scores: the laser sites had a mean score of  $5.8 \pm 0.4$  vs.  $2.0 \pm 1.2$  in the manual sites ( $p = 0.001$ ). At POD 120, the margin between laser ( $3.4 \pm 2.5$ ) and manual ( $2.8 \pm 1.3$ ) sites had narrowed considerably ( $p = 0.62$ ). Both laser and manual sites demonstrated similar pliability, with minimal hyperpigmentation and vascularity. At POD 180, there were minimal cosmetic as well as functional differences between the laser and manual sites (Figure 2). The mean Vancouver score for laser debrided sites was  $4.8 \pm 3.4$  while manually debrided sites was  $2.8 \pm 1.6$  ( $p = 0.24$ ). Both sites were devoid of hair, and possessed similar degrees of pigmentation, vascularity, pliability as well as overall scar height. When compared to the surrounding normal skin, both laser and manually debrided sites had less pliability due to scar formation, but otherwise had similar pigmentation and vascularity.

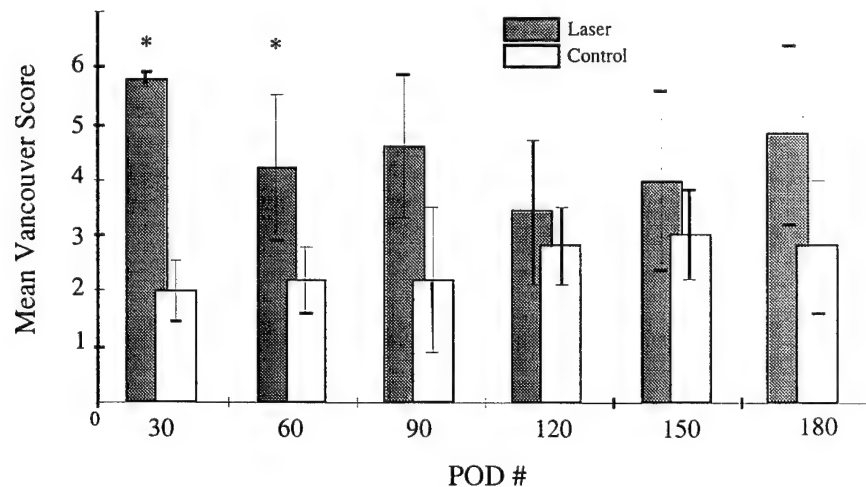


Figure 19. Vancouver Scar Assessment for laser versus manual sites followed to 6 months postgrafting. At POD 180, laser and manual sites demonstrate no statistical significance among the two groups ( $p=0.24$ ). [\*  $p < 0.05$  laser compared to manual site]

This study demonstrates that a high power, rapidly-scanned continuous wave carbon dioxide laser system can efficiently ablate full thickness burns in a porcine model and allow immediate autografting with short and long term results comparable to sharp excision. The laser ablated wounds were nearly bloodless. The ability of the laser to coagulate vessels is directly related to the degree of residual thermal damage produced after the laser interacts with the tissue. Using our system, it is expected that vessels less than 200  $\mu\text{m}$  can be coagulated [Green, 1993]. Vessels that exceed this range may require multiple scans or passes in order to achieve effective coagulation. While the purpose of this study was to compare engraftment rates rather than blood loss between laser and manual sites, it was evident that the use of the laser nearly eliminated bleeding during debridement. This has obvious implications in terms of reducing overall debridement times due to a reduction in time spent achieving hemostasis.

In general, continuous wave carbon dioxide lasers emit higher average powers than short pulse lasers. Thus, they can more rapidly remove large amounts of tissue. This is an important concern if such an instrument is to be useful to a surgeon dealing with a full thickness burn. An average power of 153 W used in our study was quite adequate for vaporizing burn eschar. Approximately 3.2 mm of tissue could be removed bloodlessly in 16 laser passes over a period of 178-228 seconds. However, as a result of using such high powers, the laser cannot be manually operated. Instead, it must be scanned across the tissue surface by a scanning system. Scanning the beam across the tissue surface also increases the inherent precision of the laser [Walsh, 1988] further reducing dwell time and subsequent thermal damage [Domankevitz, 1997].

While the thickness of granulation tissue was significantly greater in laser debrided sites during the first three months after surgery, long term examination and histology revealed no differences between the sites at 180 days. Specifically, the persistence of granulation tissue did not appear to have a significant impact on wound appearance from POD 120-180 based on Vancouver scar assessment. Similar histologic findings have been described in incisional wounds created with either carbon dioxide laser or electrocautery when compared with scalpel incisions followed to POD 42 in a miniature hairless porcine model [Pollack, 1995]. Specifically, a greater amount of granulation tissue, necrosis of the reticular dermis, and degree of foreign body granulomas were observed in laser treated sites compared with scalpel in the first 21 days. However, six weeks after incision, the laser treated wounds were histologically similar to manually incised wounds.

One limitation of this study is that the pig does not provide a good model for hypertrophic scar formation in human burn patients. Therefore, it may be difficult to extrapolate scarring outcomes seen in pigs to humans. We have started a pilot clinical study with long term follow-up to better address this issue.

In summary, laser vaporization of full thickness burn eschar was performed in eleven swine with a high power rapidly-scanned, continuous wave carbon dioxide laser with immediate engraftment that matched the sharply excised control. Residual thermal damage (180  $\mu\text{m}$ ) produced by the laser adequately limited bleeding from the wound bed without affecting split-thickness skin engraftment. Long term scarring, based on Vancouver scar assessment and histological evaluation at six months, demonstrated no clinical or statistical differences. The implications of this technology, if it can be practically and effectively brought from the laboratory into the clinical setting is a reduction in intraoperative blood loss without sacrifice of engraftment rates or cosmetic outcome. A pilot study in humans is currently underway.

#### 4. Optimize the laser ablation process by performing studies of laser ablation of skin and using theoretical models of ablation to analyze the data

Most models of pulsed infrared (IR) laser ablation of biological tissue treat tissue as a homogenous material with thermophysical properties similar to that of water. This is done despite substantial experimental evidence demonstrating that tissue mechanical properties directly affect the gross outcome of the ablation process, e.g., the efficiency of tissue removal, and the resulting tissue morphology and zone of thermal injury. The mechanical properties of biological tissue is primarily governed by a structural matrix (SM) composed of extra-cellular proteins. We therefore propose a study to examine the effect of the structural matrix on the mechanism and dynamics of the ablation process by comparing ablation events of tissue and free water. Specifically, we are making mass loss measurements in the 9.2 to 10.6  $\mu\text{m}$  wavelength range. Previous work has shown that the ablation dynamics can change depending on the tissue chromophore that is targeted. At 10.6  $\mu\text{m}$ , the dominant chromophore is water, and an explosive ablation event is observed resulting in gross tissue fracture and a layer of thermal injury of at least 150  $\mu\text{m}$ . If the wavelength is chosen such that the extracellular matrix (ECM) is targeted as the dominant chromophore and is denatured on the time scale of the laser pulse, the ablation event may be surface mediated which should decrease mechanical and thermal injury. It is possible to target both water and ECM by using the 9.6  $\mu\text{m}$  CO<sub>2</sub> laser wavelength. Comparing 9.6 and 10.6  $\mu\text{m}$  radiation should provide further insight into ablation dynamics and could lead to a more effective tissue removal process with reduced thermal damage leading to faster healing.

#### Mass Loss

The experimental setup is shown below (Figure 20). Briefly, the mass loss of tissue is measured during the ablation process and the amount of mass loss per delivered energy is determined. The crossed HeNe beams are used to accurately position the tissue surface at the focal spot of the CO<sub>2</sub> beam. The mass loss per pulse versus fluence is shown in Figure 21. The slope of the straight line fit through the data for points where plasma formation was absent represents the heat of ablation (Figure 22). Ablation efficiency is examined by comparing the mass loss at different fluences. The  $1/e^2$  heat of ablation and ablation threshold values at 10.6  $\mu\text{m}$  for porcine dermis was found to be 4.0 kJ/g and 1.2 J/cm<sup>2</sup>, respectively. The  $1/e^2$  heat of ablation and ablation threshold values at 9.6  $\mu\text{m}$  for porcine dermis was found to be 3.6 kJ/g and 1.6 J/cm<sup>2</sup>, respectively. Although the heat of ablation is higher for 10.6  $\mu\text{m}$ , at any one point the efficiency for 9.5  $\mu\text{m}$  is lower than the efficiency for 10.6  $\mu\text{m}$ .

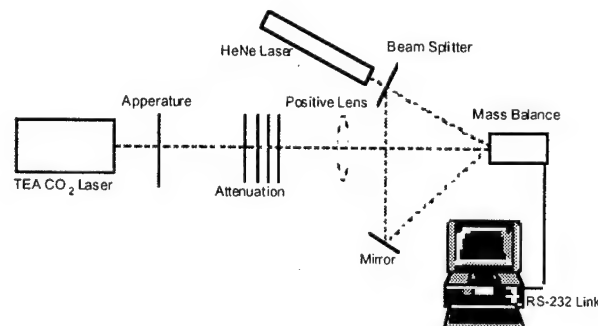


Figure 20. Experimental setup for measuring tissue mass-loss.

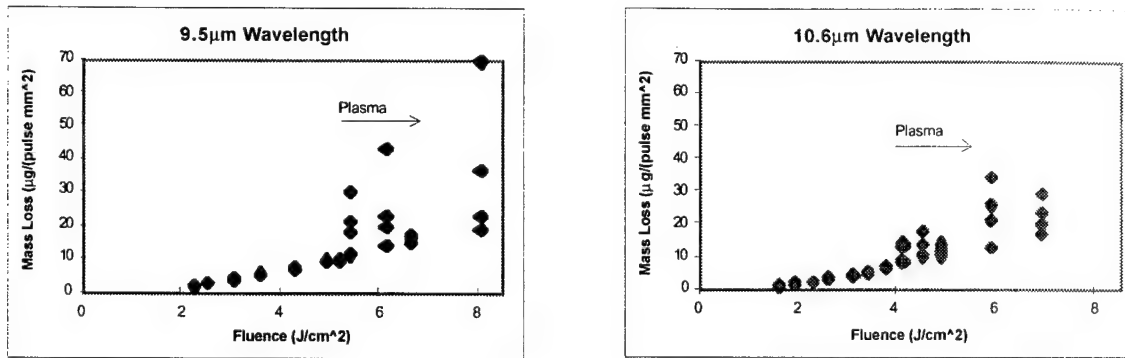


Figure 21. Mass loss versus fluence at 9.6 and 10.6  $\mu\text{m}$ .

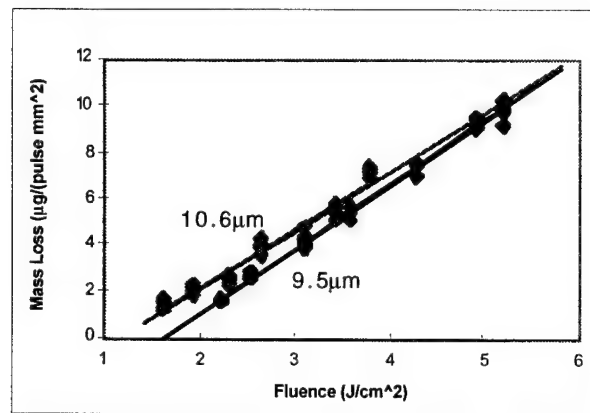


Figure 22. Heat of ablation determined from mass loss versus fluence data at 10.6  $\mu\text{m}$  to 9.6  $\mu\text{m}$ .

Although the results indicate similar mass loss characteristics for both wavelengths, there are some important differences. First, the onset of plasma formation occurs earlier for the 10.6  $\mu\text{m}$  at 4.1  $\text{J}/\text{cm}^2$  compared to 5.4  $\text{J}/\text{cm}^2$  for 9.5  $\mu\text{m}$ . This difference is probably due to higher water absorption of the 10.6  $\mu\text{m}$  wavelength. Second, in both cases plasma mediated ablation actually increases the mass loss per pulse. This effect is observed only for short pulses with symmetric energy distribution. Previous studies [e.g., Walsh, 1988] used longer pulses and thus plasma formation shielded the latter part of the pulse leading to a decrease or saturation of the mass loss per pulse. Lastly, we compare the magnitudes of mass removal with fluence to define an efficiency and heat of ablation. We make these comparisons in the regime where there is no plasma formation. If we theorize that the mechanism of ablation is more explosive at 10.6  $\mu\text{m}$  since only water absorbs the laser energy, we would expect mass removal to be more efficient due to the entrainment of solid tissue particles. At 9.5  $\mu\text{m}$  the process may be less explosive due to the denaturation of the structural matrix and thus require more energy to ablate a given mass of tissue. Although our results are consistent with our hypothesis, the slope and efficiency for both wavelengths do not differ significantly. We thus will continue our investigations using stress measurements. The increased sensitivity of measuring laser induced stresses may provide a further understanding of the ablation dynamics at these two wavelengths.

### Histology

The experimental setup and procedure for histology and assessment of thermal damage is depicted in Figure 23. The energy delivered to the tissue target was chosen based on two criteria; first, the energy was normalized with respect to the threshold measured in previous experiments and second, the energy was as high as possible without causing the onset of plasma formation. The resulting fluence at the target was 3.5  $\text{J}/\text{cm}^2$  and 4.47  $\text{J}/\text{cm}^2$  for 10.6  $\mu\text{m}$  and 9.5  $\mu\text{m}$  respectively. Fifteen samples of tissue were used at each wavelength and the number of pulses delivered to each sample was fixed at 12 (previous experiments which varied the energy and



number of pulses exhibited no significant variance in thermal damage). After laser irradiation, the tissue samples were fixed in formalin, set in paraffin, cut into 15  $\mu\text{m}$  sections and stained with hematoxylin and eosin (H&E stain).

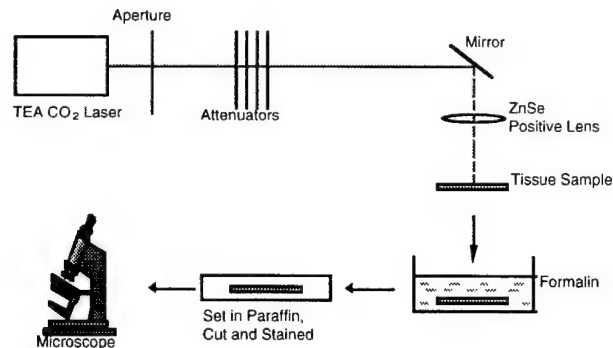


Figure 23. Illustration of histology and assessment of thermal damage procedure

The amount of thermal damage was assessed using a calibrated reticle at the center of the bottom surface of each crater to avoid edge affects. The H&E stain allowed differentiation between normal and thermally altered tissue under the microscope. At 9.5  $\mu\text{m}$ , where the dominant chromophores are the SM and tissue water, the amount of thermal damage seemed shallower and smoother compared to 10.6  $\mu\text{m}$  where the dominant chromophore is water. The average thickness of thermal damage was 75  $\mu\text{m}$  and 57  $\mu\text{m}$  with a standard deviation (STD) of 16  $\mu\text{m}$  and 12  $\mu\text{m}$  for TEA CO<sub>2</sub> irradiation at wavelengths 10.6  $\mu\text{m}$  and 9.5  $\mu\text{m}$ , respectively.

In summary, zones of thermal damage have been quantified for TEA CO<sub>2</sub> irradiation at wavelengths 10.6  $\mu\text{m}$  and 9.5  $\mu\text{m}$  [Payne, 1998]. The results show that thermal damage at 9.5  $\mu\text{m}$  irradiation is statistically lower then for 10.6  $\mu\text{m}$  irradiation. This observation is consistent with our hypothesis that thermal damage is inversely related to ablation efficiency when the ablation mechanism is the same. At 10.6  $\mu\text{m}$ , water is the dominant chromophore and thus the SM remains intact during irradiation, inhibiting material removal and causing more thermal damage. At 9.5  $\mu\text{m}$  however, the SM is compromised or weakened during irradiation thereby facilitating material removal, and consequently yielding a more efficient ablation event with lower thermal damage. In this regime, tissue chromophore and its role in preserving ultimate tensile strength appears to affect ablation dynamics, namely efficiency and level of thermal damage. This observation has significant impact for a variety of medical applications where it is advantageous to ablate thermal damage with no change in ablation mechanism. For example, CO<sub>2</sub> laser burn debridement and skin re-surfacing require approximately 80  $\mu\text{m}$  of thermal damage to cause homeostasis, however current systems often leave approximately 180  $\mu\text{m}$  of thermal damage, resulting in delayed healing. One could therefore benefit considerably by simply altering the wavelength of current systems through the utilization of a diffraction grating.

##### 5. Examine and compare various optical feedback control mechanisms including ICG fluorescence, autofluorescence and reflectance

Design of an optical feedback laser control mechanism is underway. A variety of optical techniques were investigated with the goal of identifying the transitional zone separating burn eschar from underlying healthy tissue. Specifically, fluorescence images of ICG using 780 nm and 400 nm excitation, laser-induced autofluorescence spectroscopy using 337 nm and 396 nm excitation and reflectance spectroscopy were employed. A total of 10 pigs were used in this phase of the study. Five to seven 4 x 4 cm square burn wounds were created 48 hours before laser ablation. On POD #0 (PBD #2) the surface of the burns were removed via 0, 2, 4, 6, 8, and 10 laser passes using the therapeutic laser system with a 1.4 mm spot diameter, 35 J/cm<sup>2</sup> and 0.7 mm line spacing. Following laser ablation, each burn site was measured using the optical techniques listed above. For recording fluorescence images, 0.2 mg/kg of ICG was given intravenously. To prevent distortion of the other



optical techniques due to the added ICG, the imaging measurements are performed last. The ablated area was oversized relative to the burn to permit measurements of normal tissue as the upper layers are removed. Biopsies are taken and used to fine tune the laser parameters. Following measurements, the control site (received 0 passes) was mechanically débrided and all sites were grafted using 2:1 meshed, split thickness skin grafts. The viability of the grafts are evaluated visually and with biopsies on days 7 and 14. The number of passes and measurement techniques used for the 10 animals are shown in Table 4. Sites where grafting was successful are denoted with the number of laser passes given in boldface. Graft take was assessed histologically from biopsies taken on POD 5. Positive graft take specimens display a healthy epidermis and a well-defined graft dermis to host dermis junction. Inflammatory infiltrate is generally present at the junction. When these characteristics are present throughout the biopsy specimen, the site is given a “++” score. Occasionally, the junction is missing in a portion of the biopsy which we attribute to the meshing of the graft. These sites are generally marked as “+” because most of the biopsy sample displays positive graft take properties. Sites marked as “-” generally displayed a necrotic epidermis or a healthy epidermis but lack the dermo-dermal junction indicating that healing originated from secondary processes such as from the deep follicle buds. The percent wound coverage measured from photographs at POD 14 was also used in graft-take assessment although to a lesser extent. The photos are generally used to assess how well the POD 5 and POD 14 biopsy sites represent the entire wound site. Typically, positive results from biopsies must represent an area of coverage greater than or equal to 50%. However, coverage is sometimes difficult to assess because in some cases a thin shell of necrotic tissue (“onion skin”) exists as the most superficial layer that if removed will reveal a well healed graft site below. In these cases, photos from POD 21 are also used to differentiate onion skin from crust associated with an unhealed site because generally, the onion skin is absent at POD 21 whereas the crust is not.

Table 4. Graft take results and optical techniques used in the optical feedback experiments. The boldface number of passes denote site where graft take was positive.

Pig #	Passes	IR ICG Images	UV ICG Images	337 nm LIF	396 nm LIF	Reflectance
1	0, 2, 4, <b>6</b> , 8	x		x		
2	0, 4, 5, 6, 7	x	x	x	x	x
3	0, 4, 5, <b>6</b> , 7	x		x	x	x
4	0, 2, 4, <b>6</b> , 8, 10	x	x	x	x	x
5	0, 2, 4, 6, <b>6</b> , 8, 10	x	x	x	x	x
6	0, 2, 4, <b>6</b> , <b>6</b> , 8, 10	x	x	x	x	x
7	0, 2, 4, 6, 8, 10		x	x	x	x
8	0, 4, <b>6</b> , 8, 10		x	x	x	x
9	0, 2, 4, <b>6</b> , 8, 10		x	x	x	x
10	0, 2, 4, 6, 8, 10		x	x	x	x

The 337 nm LIF, 396 nm LIF, and reflectance techniques are point measurement made with fibers placed in contact with the tissue using the arrangement presented in Figure 24. Six measurements were made in the ablated normal area (lighter zone) and 9 made in the ablated burn injured region (darker zone). For further processing the mean spectra recorded inside and outside the burn area were used. The IR and UV induced ICG fluorescence images were quantitated in an analogous manner by defining regions of interest (ROI) at the selected 15 sites. Each technique was evaluated on an absolute sense using measured intensities found in the burn injured region and on a relative sense by referencing to the values from in the ablated normal area.

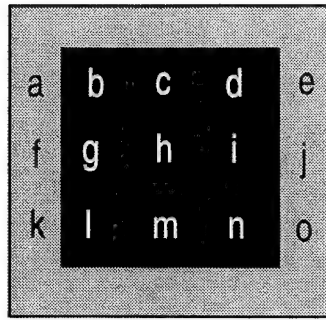


Figure 24. Measurement scheme for point measurement techniques.

Each optical technique was individually assessed for its ability to predict graft take using a multivariate linear regression (MVLR) analysis,

$$MVLR \text{ Score}_j = a_0 + \sum_i a_i I_j(\lambda_i). \quad (11)$$

Briefly, each spectrum,  $I_j$ , is classified into either a positive or negative graft-take group and assigned scores of +1 or -1, respectively, depending on whether graft take was positive or negative. A stepwise MVLR analysis is performed, where coefficients,  $a_i$ , are determined to best predict assigned scores. The method is stepped to drops variables,  $I_j(\lambda_i)$ , which insignificantly contribute to the scores. The sensitivity, specificity, predictive value positive and accuracy of each optical technique and are given in Table 5.

Table 5. Statistical outcome of each diagnostic technique for predicting graft take.

Optical Technique	Variables	Sensitivity	Specificity	Predictive Value Positive	Accuracy
IR/ICG	Constant	38%	76%	48%	62%
	IRICGin				
UV/ICG	Constant UVICGin/ UVICGout	50%	65%	60%	61%
Reflectance	Constant I(420), I(520)	91%	80%	83%	83%
337 LIF	Constant	73%	71%	67%	71%
	I(420), I(490)				
	I(530), I(690)				
396 LIF	Constant	73%	71%	67%	71%
	I(680), I(700)				

Reflectance spectroscopy was most sensitive in predicting graft outcome taking the predictive value positive is the more pertinent decisor in this application because it decide when the laser has ablated deep enough to produce a graft-acceptable bed. In other words, what percentage of site marked as graftable by the diagnostic went on to achieve successful graft-take. As expected, the IR-induced ICG fluorescence technique is a poor predictor of a graftable bed because the relatively large penetration of 780 nm light makes it insensitive to changes occurring in the first 100-200  $\mu\text{m}$  from the surface. A range of PVP from 48% to 83% using MVLR

analysis was obtained from the other optical techniques. The reflectance algorithm was sensitive to measurement at 420 and 520 nm. The reflectance at 420 nm reflects changes in the amount of hemoglobin present, whereas the 520 nm is most likely probing shifts in the baseline as the result of changes in the scattering properties of the tissue. Typically, there is a higher relative hemoglobin content in sites where grafts took which may be related to the zone of stasis.

Using tissue reflectance at 420 and 520 nm, Figure 25 shows a band of enhanced hemoglobin absorption in burn tissue. The placement of split thickness skin graft on the peak of this band should be beneficial to healing outcome. Although using visual guidance, burn debridement stopped after 16 laser passes, the reflectance algorithm predicts that burn debridement should have stopped after 8 laser passes conserving substantial amounts of tissue (ca. 8 passes x 0.22 mm per pass or 1.8 mm). This is the difference between placing the graft on dermal or adipose tissue, respectively. It should be noted that the actual burn depth based on tissue stained for lactate dehydrogenase activity is 2.7 mm. It should also be noted that optical density is a log scale implying a 10 to 100-fold difference comparing ablated burn to ablated normal tissue after 8 laser passes.

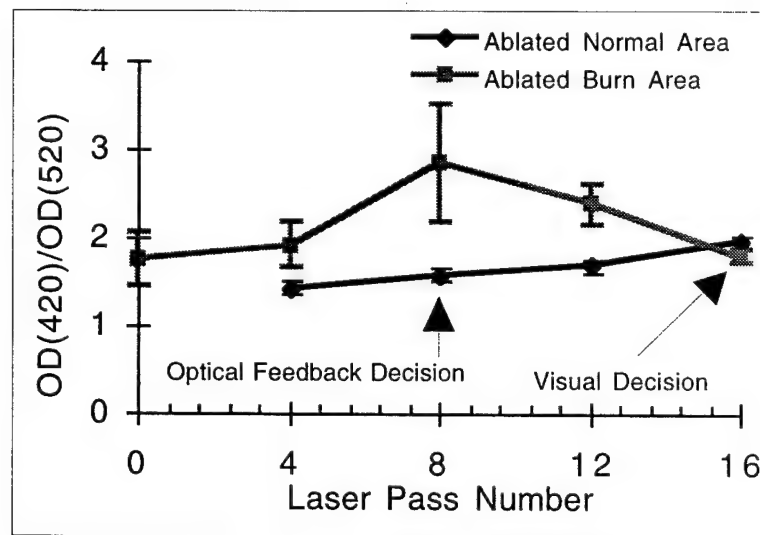


Figure 25. Graft placement using reflectance feedback algorithm.

In summary, reflectance spectroscopy may be useful as a feedback control mechanism for informing the therapeutic laser to stop ablating at the transitional plane lying between burn eschar and underlying healthy tissue. The reflectance algorithm is presently being tested in a prospective study. Currently 4 animals have been studied to date. Early results show similar percent engraftment independent of visual or reflectance guided feedback, however 2 to 3 less laser passes are required under reflectance control.

#### 6. Familiarize medical personnel from military and civilian hospitals in the use of the system in preparation for clinical testing

Dr. Sheridan from the Shriners' Burns Institute in Boston has been instructed in the safe use of the Tx1A system and is quite familiar with operating it. Dr. Sheridan has initiated an independent clinical trial using a commercial CO<sub>2</sub> laser system (Surgilase 150XL, Sharplan Laser Inc). The pilot study has enrolled 21 patients to date and is intended to show feasibility of laser debridement in humans. Graft sites were monitored up to one year. The results from the human study confirms our results found in pigs [Sheridan, 1998]. In particular, bloodless debridement is possible with lasers with equivalent percent engraftment and one year Vancouver Scar scores comparing laser ablated sites to control sites. However, breakthrough bleeding was noted in two older granulated wounds. Further work is continuing evaluating operating time and subsets of burns most suitable for laser debridement.

Plans are underway to evaluate the feasibility of using the TX1A laser system for treating chemical burns. The intent is to debride deep wounds induced by sulfur-mustard vapor through a Scientific and Technical Analysis Services (STAS) contract with John Graham at the US Army Medical Research Institute of Chemical Defense. The protocol is design to test our high-power rapidly-scanned debridement system with a commercially available medical CO<sub>2</sub> laser.

*7. Construct a second prototype system for testing at a second clinical site*

The design of a second generation burn debridement laser system has been completed and documented via a Cooperative Research and Development Agreement (CRADA No. SC93/01177) with Sandia National Laboratories. The prototype completely integrates the burn diagnostic and therapeutic system and has more advanced safety features. Details of this system are available from Sandia National Laboratories: Sandia Report SAND96-2327.UC-700, Final Report for the Burn Diagnostic and Laser Debridement Project.

## CONCLUSIONS

In conclusion, we have made substantial progress in all objectives. We have constructed and tested a diagnostic technique that uses ICG fluorescence to determine burn depth. The technique was shown to be successful in assessing burn depth in small and large animals [Green, 1992a; Jerath, 1998]. The distribution of ICG into burns and normal tissue was studied to assist in deriving the segmentation algorithms [Schomacker, 1997]. The technique was also safely used in a pilot clinical trial [Sheridan, 1995]. However, the clinical trial has shown that skin type and antimicrobial agents affect measurements. We believe these changes can be accounted for by monitoring how the intensity of ICG fluorescence changes over the first 10 minutes following intravenous injection. Further studies examining this concept are in progress with collaboration with Star Medical Technologies, Inc. SMT has developed a small portable ICG imager using high-power laser diodes and is also testing the system for evaluating skin flaps and ulcers. Laser speckle was evaluated successfully in a Teflon phantom model mimicking burns [Sadhvani, 1996] and more recently in porcine skin burns [Fike, In prep]. In addition, a laser burn debridement system was constructed and tested on porcine skin burns [Lucchina, 1993; Glatter, 1998]. Burns were tangentially excised bloodlessly and equivalent percent engraftment rates and Vancouver scar scores were obtained comparing laser debrided sites to sharply-excised controls. This was the first study to report successful grafting following burns excision with continuous wave CO<sub>2</sub> laser. The system employs a high-power, rapidly-scanned cw carbon dioxide laser which was shown to be able to control the amount of residual thermal damage [Domankevitz, 1997]. These observations have just recently been confirmed in human burns [Sheridan, submitted] and were presented at the 50<sup>th</sup> Anniversary of the US Army Medical Research Institute for Surgical Research. The laser debridement system was also used to excise chronic intradermal adriamycin wounds mimicking chemical burns and further plans are underway to evaluate its efficacy in excising sulfur-mustard wounds in pigs through collaboration with the US Army Medical Research Institute for Chemical Defense. Progress has been made in developing a feedback control mechanism for controlling the laser debridement system. Identifying the transition zone between burn eschar and underlying healthy tissue is possible using reflectance spectroscopy. The technique is presently being tested in a prospective study using a porcine skin burn model. Early results are quite promising with no difference observed in percent engraftment rates comparing laser excised burns sites under visual and feedback-controlled guidance. Finally, a more elegant laser debridement burn diagnostic robotic system (Prototype II) has been designed via a cooperative research agreement with Sandia National Laboratories (CRADA SC93/01177, Sandia Report SAND96-2327). Construction of this system could occur via an industrial partner, once laser debridement is accepted as a safe alternative to standard burn escharectomy offering more efficient, precise and bloodless excision of burns.

## REFERENCES

- Aach Rd, Stevens CE, Hollinger FB, et al. Hepatitis C virus infection in post-transfusion hepatitis. An analysis with first-and second-generation assays. *New Engl J Med* 1991; 325: 1325-1329.
- Afromowitz MA, Van Liew GS, Heimbach D. Clinical evaluation of burn injuries using an optical reflectance technique. *IEEE Trans Biomed Eng* 1987;34(2):114-117.
- Afromowitz MA, Callis JB, Heimbach DM, DeSoto LA, Norton MK. Multispectral imaging of burn wounds: a new clinical instrument for evaluating burn depth. *IEEE Trans Biomed Eng* 1988;35(10):842-850.
- Anderson RR, Parrish JA. The optics of human skin. *J Inv Derm* 1981;77(1):13-19.
- Anderson RR and Parrish JA. Optical Properties of Human Skin. In Regan JD, Parrish JA, eds. *The Science of Photomedicine*, New York: Plenum, Press, 1982: 147-164.
- Atilas L, Mileski W, Spann K, Purdur G, Hunt J, Baxter C. Early assessment of pediatric burn wounds by laser Doppler flowmetry. *J Burn Care Rehabil* 1995; 16: 596-601.
- Baker KJ. Binding of sulfobromophthalein and indocyanine green by plasma  $\alpha_1$ -lipoproteins. *Proc Soc Exp Biol (NY)* 1966; 122: 957-63.
- Balogh K, Dudley HR, Cohen RB. Oxidative Enzyme Activity in skeletal cartilage and bone. *Lab Invest* 1961; 10: 838-845.
- Barnes RB. Thermography of the human body. *Science* 1963;140:870-877.
- Bauer JA, Sauer T. Cutaneous 10 MHz ultrasound B scan allows the quantitative assessment of burn depth. *Burns* 1989;15(1):49-51.
- Bennett JE, Dingman RO. Evaluation of burn depth by the use of radioactive isotopes-an experimental study. *Plas Reconstr Surg* 1957;20(4):261-272.
- Benson RC and Kues HA. Fluorescence properties of indocyanine green as related to angiography. *Phys Med Biol* 1978; 3: 159-63.
- Black KS, Hewitt CW, Miller DM, Ramos E, Halloran J, Bressler V, Martinez SE, Achauer BM. Burn depth evaluation with fluorometry: Is it really definitive? *J Burn Care Rehabil* 1986; 7: 313-317.
- Boas DA and Yodh AG. Spatially varying dynamical properties of turbid media probed with diffusing temporal light correlation. *J Opt Soc Am A* 1997; 14: 192-215.
- Briers JD and Fercher AF, Retinal Blood-Flow Visualization By Means Of Laser Speckle Photography, *Invest. Ophthalmol. Vis. Sci.* 1982; 22: 255-259.
- Buecker JW, Ratz JL, Richfield DF. Histology of port-wine stain treated with the carbon dioxide laser. *J Am Acad Dermatol* 1984; 10: 1014-1019.
- Buell BR, Schuller DE. Comparison of tensile strength in CO<sub>2</sub> laser and scalpel skin incisions. *Arch Otolaryngol* 1983; 109: 465-467.
- Cantrell JH, Yost WT. Can ultrasound assist an experienced surgeon in estimating burn depth? *J Trauma* 1984;24(9S):64-70.
- Cherrick GR, Stein SW, Leevy CM, Davidson CS. Indocyanine green: observations on its physical properties, plasma decay, and hepatic extraction. *J Clin Invest* 1960;39:592-600.
- Cheong WF, Prahl SA, Welch AJ, A review of the optical properties of biological tissue, *IEEE J. Quant. Electron.* 1990; 26 : 2166-2185.
- Cole RP, Jones SG, Shakespeare PG. Thermographic assessment of hand burns. *Burns* 1990;16:60-63.
- Cope O, Langohr JL, Moore FD, Webster RC. Expeditious care of full-thickness burn wounds by surgical excision and grafting. *Ann Surg* 1947;125(1):1-22.

- Demling RH, LaLonde C. Early wound excision and grafting. In: Burn Trauma, New York, Thieme Medical Publishers, Inc., 1989:118-145.
- Desai MH, Herndon DN, Broemeling L, Barrow RE, Nichols RJ, Jr., Rutan RL. Early burn wound excision significantly reduces blood loss. *Ann Surg* 1990; 211: 753-759.
- Dingwall JA. A clinical test for differentiating second from third degree burns. *Ann Surg* 1943;118(3):427-429.
- Domankevitz Y, Nishioka NS. Effects of a rapidly-scanned carbon dioxide laser on porcine dermis. *J Burn Care Rehabil* 1997; 18: 206-209.
- Farrell TJ, Patterson MS, Wilson B, A diffusion theory model of spatially resolved, steady-state diffuse reflectance for the noninvasive determination of tissue optical properties *in vivo*, *Med. Phys.* 1992; 19: 879-888.
- Fercher AF and Briers JD, Flow Visualization By Means Of Single-Exposure Speckle Photography, *Opt. Commun.* 1981; 37: 326-330.
- Fidler JP. Techniques of laser burn surgery. In: Goldman, editor. *The Biomedical Laser: Technology and Clinical Applications*. New York: Springer-Verlag, 1981: 199-218.
- Fidler JP, Bendick PJ, Glover JL, Holder IA. Effects of CO<sub>2</sub> laser on wound healing and infection. *Lasers Surg Med* 1983; 3: 109, Abstract 17.
- Fike EE, Schomacker KT, Glatter RD, Nishioka NS. Determination of Burn Depth using Laser Speckle in a Porcine Burn Model. In prep. Flemming AF, Frame JD, Dhillon R. Skin edge necrosis in irradiated tissue after carbon dioxide laser excision of tumor. *Lasers Med Sci* 1986; 1: 263-265.
- Fox IJ, Brooker LGS, Wood EH. A new dye for continuous recording of dilution curves in whole blood independent of variations in blood oxygen saturation. *Circulation* 1956;14:937-938.
- Fry TL, Gerbe RW, Botros SB, Fischer ND. Effects of laser, scalpel, and electrosurgical excision on wound contracture and graft "take". *Plast Reconstr Surg* 1980; 65: 729-731.
- Gatti JE, LaRossa D, Silverman DG, Hartford CE. Evaluation of the burn wound with perfusion fluorometry. *J Trauma* 1983;23(3):202-206.
- Gillis TM, Strong MS. Surgical lasers and soft tissue interactions. *Otolaryngol Clin North Am* 1983; 16: 775-784.
- Goodman JW, "Statistical Properties of Laser Speckle Patterns," in Laser Speckle and Related Phenomena. Dainty JC, ed., Springer-Verlag, New York, 1975: 12.
- Graves TA, Cioffi WG, Mason AD, Jr., McManus WF, Pruitt BA, Jr. Relationship of transfusion and infection in a burn population. *J Trauma* 1989; 29: 948-952.
- Gray DT, Early surgical excisions versus conventional therapy in patients with 20-40% burns, *Amer. J. Surg.* 1982; 144: 76-80.
- Green DM and Diller KR. Measurement of burn-induced leakage of macromolecules in living tissue. *J Biomech Eng* 1978; 100: 153-158.
- Green HA, Bua D, Anderson RR, Nishioka NS. Burn depth estimation using indocyanine green fluorescence. *Arch Dermatol* 1992a; 128: 43-9.
- Green HA, Bua D, Nishioka NS, Bruggemann U, Compton CC. Mid-dermal wound healing: A comparison between dermatomal excision and pulsed carbon dioxide laser ablation. *Arch Dermatol* 1992b; 128: 639-645.
- Green HA, Burd EE, Nishioka NS, Compton CC. Skin graft take and healing following 193-nm excimer, continuous-wave carbon dioxide, pulsed CO<sub>2</sub>, or pulsed Holmium:YAG laser ablation of the graft bed. *Arch Derm* 1993; 129: 979-988.
- Groves AR, Lawrence JC. The tangential excision of burns: an experimental study using an animal model. *Injury* 1971;3(1):30-39.

- Hall RR. The healing of tissues incised by a carbon dioxide laser. *Brit J Surg* 1971; 58: 222-225.
- Hambley R, Hebda PA, Abell E, Cohen BA, Jegasothy BV. Wound healing of skin incisions produced by ultrasonically vibrating knife, scalpel, electrosurgery, and carbon dioxide laser. *J Dermatol Surg Oncol* 1988; 14: 1213-1218.
- Hartford CE, McClellan RM. Tangential Excision of the burned hand with immediate skin grafting [movie] Produced by CE Hartford. Chester, Pa: Chester Medical Center Burn Unit, 1980.
- Hauben DJ, Mahler D. Histological investigation of burn eschar and the underlying recipient area in tangential early excision of burns. *Burns* 1979;5:160-163.
- Hebda H, et al. Basic Fibroblast Growth Factor Stimulation of Epidermal Wound Healing in Pigs. *J Invest Derm* 1990; 95: 626-631.
- Heimbach D, Engrav L, Grube B, Marvin J. Burn depth: a review. *World J Surg* 1992; 16: 10-5.
- Henriques FC and Moritz AR. The conduction of heat to and through skin and the temperatures attained therein. A theoretical and an experimental investigation. *Am J Path* 1947; 23: 531-549.
- Hlava P, Moserova J, Konigova R. Validity of clinical assessment of the depth of a thermal burn. *Acta Chir Plast* 1983; 25: 202-208.
- Hukki JH, Lapasti J, Castren M, Puolakkainen P, Schroder T, Lactate Dehydrogenase in Laser Incisions: A Comparative Analysis of Skin Wounds Made With Steel Scalpel, Electrocautery, Superpulse-Continuous Wave Mode Carbon-Dioxide Lasers, and Contact Nd:YAG Laser, *Lasers Surg. Med.* 1989; 9: 589-594.
- Jackson DM. The diagnosis of the depth of burning. *Br J Surg* 1953; 40: 588-96.
- Jackson DM. Second thoughts on the burn wound. *J Trauma* 1969; 9(10): 839-62.
- Jackson DM. Historial review of the use of local physical signs in burns. *Br J Plas Surg* 1970a;23(3):211-218.
- Jackson DM. In search of an acceptable burn classification. *Br J Plas Surg* 1970b;23(3):219-226.
- Jackson DM, Stone PA. Tangential excision and grafting of burns. *Br J Plas Surg* 1972;25:416-426.
- Jackson DM. The William Gissane Lecture 1982: The burn wound: its character, closure and complications. *Burns* 1982;10:1-8.
- Janzekovic Z. A new concept in the early excision and immediate grafting of burns. *J Trauma* 1970;10(12):1103-1108.
- Jarmuske MB, Stranc MF, Stranc LC. The effect of carbon dioxide laser on wound contraction and epithelial regeneration in rabbits. *Br J Plast Surg* 1990; 43: 40-
- Jerath MR, Schomacker KT, Nishioka NS. Estimation of the Extent of Burn Injury using Indocyanine Green Fluorescence. *J Trauma* 1998, In Prep.
- Kalus AM. Application of ultrasound in assessing burn depth. *Lancet* 1979;188-189.
- Keijzer M, Richards-Kortum RR, Jacques SL, Feld MS, Fluorescence spectroscopy of turbid media: Autofluorescence of the human aorta, *Appl. Opt.* 1989; 28: 4286-4292.
- Landsmann MLJ, Kwant G, Mook GA, Zijlstra WG. Light-absorbing properties, stability, and spectral stabilization of indocyanine green. *J Appl Physiol* 1976; 40: 575-83.
- Lawrence JC, Carney SA. Tangential excision of burns: studies on the metabolic activity of the recipient areas for skin grafts. *B J Plas Surg* 1973;26:93-100.
- Levine NS, Ger R, Stellar S, Levenson SM. Use of a Carbon Dioxide Laser for the Debridement of Third Degree Burns. *Ann Surg* 1972; 179: 246-252.
- Levine NS, Salisbury RE, Peterson HD, Pruitt BA, Jr. Clinical evaluation of the carbon dioxide laser for burn wound excisions: a comparison of the laser, scalpel, and electrocautery. *J Trauma* 1975; 15: 800-807.



- Levine NS, Peterson HD, Salisbury RE, Pruitt BA, Jr. Laser, scalpel, electrosurgical, and tangential excisions of third degree burns. A preliminary report. *Plast Reconstr Surg* 1975; 56: 286-296.
- Levine BA, Sirinek KR, Pruitt, BA.. Wound excision to fascia in burn patients. *Arch Surg* 1978;113:403-407.
- Lucchina LC, Bua DP, Domankevitz Y, Silver GM, Sheridan RL, Nishioka NS. High power carbon dioxide laser ablation and split-thickness skin grafting of burn wounds. Presented at the Society Invest Dermatol 1994. *J Invest Dermatol* 1994; 102: 602 (Abstract 471).
- MacMillan, B. Determining the depth of injury. *J Trauma* 1979;19(11s):927.
- Mann R, Heimbach DM, Engrav LH, Foy H. Changes in transfusion practices in burn patients. *J Trauma* 1994; 37: 220-222.
- Marano MA, O'Sullivan G, Madden M, Finkelstein J, Goodwin CW. Tourniquet technique for reduced blood loss and wound assessment during excisions of the extremity. *Surg Gyn Obstet* 1990; 171: 249-250.
- McKenzie AL. How far does thermal damage extend beneath the surface of the CO<sub>2</sub> laser incisions? *Phys Med Biol* 1983; 28: 905-912.
- Michaels J, Alsbjorn B, Sorensen B. Clinical use of laser doppler flowmetry in a burns unit. *Scan J Plast Reconstr Surg* 1984;18:65-73.
- Mladick R, Georgiade N, Thorne F. A clinical evaluation of the use of thermography in determining degree of burn injury. *Plast Reconstr Surg* 1966;38(6):512-518.
- Moes CJM, van Gemert MJC, Star WM, Marijnissen JPA, Prahl SA, Measurements and calculations of the energy fluence rate in a scattering and absorbing phantom at 633 nm, *Appl. Opt.* 1989; 28: 2292-2296.
- Montagna W et al. The Skin of the Domestic Pig. *J Invest Derm* 1964; 64: 11-
- Montgomery TC, Sharp JB, Bellina JH, Ross LF. Comparative gross and histological study of the effects of scalpel, electric knife, and carbon dioxide laser on skin and uterine incisions in dogs. *Lasers Surg Med* 1983; 3: 9-22.
- Moreno RA, Hebda PA, Zitelli JA, Abell E. Epidermal cell outgrowth from CO<sub>2</sub> laser and scalpel cut explants: implications for wound healing. *J Dermatol Surg Oncol* 1984; 10: 863-868.
- Moritz AR. Studies of thermal injuries. III. The pathology and pathogenesis of cutaneous burns. An Experimental Study. *Am J Pathol* 1947; 23: 915-941.
- Morris JA, Jr., Wilcox TR, Reed GW, et al. Safety of the blood supply. Surrogate testing and transmission of hepatitis C in patients after massive transfusion. *Ann Surg* 1994; 219: 517-25.
- Newman P. A practical technique for the thermographic estimation of burn depth: a preliminary report. *Burns* 1980;8:59-63.
- Niazi ZB, Essex TJ, Papini R, Scott D, McLean NR, Black MJ. New laser Doppler scanner, a valuable adjunct in burn depth assessment. *Burns* 1993; 19: 485-9.
- Nishioka NS, Domankevitz Y, Flotte TJ, Anderson RR. Ablation of rabbit liver, stomach and colon with a pulsed holmium laser. *Gastroenterology* 1989;96:831-837.
- Payne BP, Nishioka NS, Mikic BB, Venugopalan V. Comparison of Pulsed Laser Ablation at 10.6 and 9.5  $\mu$ m. *Lasers Surg Med* 1998; 23: in press
- Parry G. Speckle patterns in partially coherent light. In: *Laser Speckle and Related Phenomenon*. Dainty JC, ed. Springer Verlag:New York, pp. 78-121, 1975.
- Pollack SV, Hurwitz JJ, Bunas SJ, Manning T, McCormack KM, Pinnell SR. Comparative study of wound healing in porcine skin with CO<sub>2</sub> laser and other surgical modalities: Preliminary findings. *Intl J Dermatol* 1995; 34: 42-47.

- Prahl SA, van Gemert MJC, Welch AJ. Determining the optical properties of turbid media by using the adding-doubling method, *Appl. Opt.* 1993; 32: 559.
- Rapaport E, Ketterer SG, Weigand BD. Hepatic clearance of indocyanine green. *Clin Res* 1959;7:289-290.
- Roberts AH. The effect of topical epinephrine on blood loss following tangential excision of burn wounds [letter]. *Plast Reconstr Surg* 1984; 74: 450-451.
- Robinson NB, Heimbach DM, Reynolds LO, et al. Ventilation and perfusion alterations following homologous blood transfusion. *Surgery* 1982; 92: 183-191.
- Rosenberg JL and Zawacki BE. Reduction of blood loss using tourniquets and "compression" dressings in excising limb burns. *J Trauma* 1986; 26: 47-50.
- Ruth B, Superposition of two dynamic speckle patterns, *J. Modern Opt.* 1992; 39: 2421-2436.
- Sadhwani A, Schomacker KT, Tearney GJ, Nishioka NS. Determination of Teflon thickness with laser speckle. I. Potential for burn depth diagnosis. *Appl Optics* 1996; 35: 5727-35.
- Schomacker KT, Walsh JT, Flotte TJ, Deutsch TF. Thermal Damage produced by high-irradiance continuous wave CO<sub>2</sub> laser cutting of tissue. *Lasers Surg Med* 1990; 10: 74-84.
- Schomacker KT, Torri A, Sandison DR, Sheridan RL, Nishioka NS. Biodistribution of indocyanine green in a porcine burn model: light and fluorescence microscopy. *J Trauma* 1997; 43: 813-819.
- Sheridan RL, Tompkins RG, Burke JF. Management of burn wounds with prompt excision and immediate closure. *J Int Care Med* 1994; 9: 6-19.
- Sheridan RL, Schomacker KT, Lucchina LC, Hurley J, Yin LM, Tompkins RG, Jerath M, Torri A, Greaves KW, Bua BS, Nishioka NS. Burn depth estimation by use of indocyanine green fluorescence: initial human trial. *J Burn Care Rehabil* 1995; 16: 602-4.
- Sheridan RL, Petras L, Glatter RD, Schomacker KT, Tompkins RG. *Surgery* 1998, submitted.
- Siegal RJ, Vistnes LM, Iverson RE. Effective hemostasis with less epinephrine. *Plast Reconstr Surg* 1973; 51: 129-133.
- Sittig KM and Deitch EA. Blood transfusions: for the thermally injured or for the doctor? *J Trauma* 1994; 36: 369-372.
- Slutzki S, Shafir R, Bornstein LA. Use of the carbon dioxide laser for large excisions with minimal blood loss. *Plast Reconstr Surg* 1977; 60: 250-255.
- Snelling CFT and Shaw K. The effect of topical epinephrine hydrochloride in saline on blood loss following tangential excision of burn wounds. *Plast Reconstr Surg* 1983; 72: 830-834.
- Solomon JR. Early surgical excision and grafting of burns including tangential excision. *Progress in Pediatric Surgery* 1981;14:133-149.
- Stuart JD, Kenney JG, Lettieri J, et al. Application of single-donor fibrin glue to burns. *J Burn Care Rehabil* 1988; 9: 619-622.
- Sullivan T, Smith J, Kermode J, McIver E, Courtemanche DJ. Rating the Burn Scar. *J Burn Care Rehabil* 1990; 11: 256-260.
- Swindle MM et al. Porcine Models in Surgical Research: An Overview. In *Swine in Biomedical Research*, in Tumbleson (Ed) 1986; 64: 235-251.
- Tompkins RG, Burke JF, Schoenfeld DA, Bondoc CC, Quinby WC Jr, Behringer GC, Ackroyd FW. Prompt eschar excision: a treatment system contributing to reduced burn mortality. A statistical evaluation of burn care at the Massachusetts General Hospital (1974-1984). *Ann Surg* 1986; 204: 272-281.
- Tompkins RG, Schoenfeld DA, Behringer GC, Bondoc CC, Ackroyd FW, Quinby WC, Burke JF. Prompt eschar excision: a treatment system contributing to reduced burn mortality. *Ann Surg* 1987;204(3):272-281.

Wachtel TK, Leopold GR, Frank HA, Frank DH. B-mode ultrasonic echo determination of depth of thermal injury. *Burn* 1986;12:432-437.

Walsh JT, Flotte TJ, Anderson RR, Deutsch TF. Pulsed CO2 laser Tissue Ablation: Effects of Tissue Type and Pulse Duration on Thermal Damage. *Lasers Surg Med* 1988; 8: 108-118.

Waxman K, Lefcourt N, Achauer B. Heated laser doppler flow measurements to determine depth of burn injury. *Am J Surg* 1989; 157:541-543.

Waymack JP, Fernandes G, Cappelli PJ, et al. Alterations in host defense associated with anesthesia and blood transfusions. II. Effect on response to endotoxin. *Arch Surg* 1991; 126: 59-62.

Wilhelm DL and Mason B. Vascular permeability changes in inflammation: the role of endogenous permeability factors in mild thermal injury. *Br J Exp Pathol* 1960; 61: 487-506.

Wilson BC, Jacques SL. Optical reflectance and transmittance of tissues: principles and applications. *IEEE J Quant Elec*, in press.

Yeong EK, Mann R, Goldberg M, Engrav L, Heimbach D. Improved accuracy of burn wound assessment using laser Doppler. *J Trauma* 1996; 40: 956-61.

**Personnel:**

Principal Investigator:	John A. Parrish, M.D.
Consultant:	Ronald Tompkins, M.D., Ph.D.
Investigators:	Norman S. Nishioka, M.D.
	Robert L. Sheridan, M.D.
	Rox R. Anderson, M.D.
	Maya Jerath, Ph.D.
	Kevin T. Schomacker, Ph.D.
	Rob Webb, Ph.D.
	Vasan Venugopalan, Sc.D.
Clinical Research Fellows:	Geoffrey Silver, M.D.
	Leslie C. Lucchina, M.D.
	Andrea Torri, M.D.
	Julie S. Goldberg, M.D.
	Robert D. Glatter, M.D.
Engineers:	Dominic Bua
	Yacov Domankevitz
	Kenneth Greaves
	Ed Hanel
Research Nurse:	Jane Hurley, R.N.
Pathologist:	Thomas J. Flotte, M.D.
Histology Technicians:	Katherine Roberts
	Bart Johnson
Students:	Ajay Sadhwani
	Eugene E. Fike
	Barry P. Payne
Secretaries:	Sandy Steinmetz
	Nancy Radford
Administrator:	Susan Weeks

**Publications:**

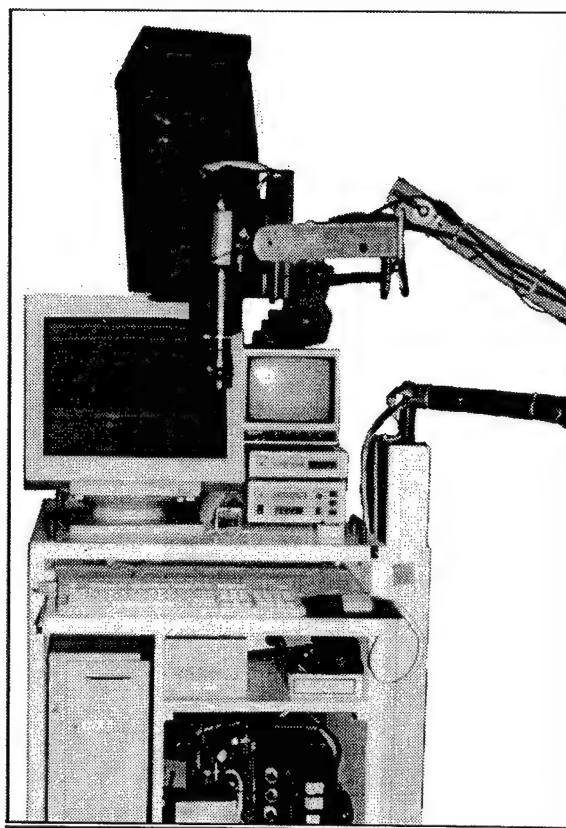
1. Sheridan RL, Schomacker KT, Lucchina LC, Hurley J, Yin LM, Tompkins RG, Jerath M, Torri A, Greaves KW, Bua DP, Nishioka NS. Burn Depth Estimation by Use of Indocyanine Green Fluorescence: Initial Human Trial. *J Burn Care Rehabil* 1995; 16: 602-604.
2. Venugopalan V, Nishioka NS, Mikic BB. The Thermodynamic Response of Soft Biological Tissue to Pulsed Infrared-Laser Irradiation. *Biophys J* 1996; 69: 1259-1271.
3. Sadwani A, Schomacker KT, Tearney GJ, Nishioka NS. Determination of Teflon Thickness using Laser Speckle. I. Potential for Burn Depth Diagnosis. *Appl Opt* 1996; 35: 5727-5735.
4. Domankevitz Y, Nishioka NS. Effects of a Rapidly Scanned Carbon Dioxide Laser on Porcine Dermis. *J Burn Care Rehabil* 1997; 18: 206-209.
5. Schomacker KT, Torri A, Sandison DR, Sheridan RL, Nishioka NS. Biodistribution of Indocyanine Green in a Porcine Burn Model: Light and Fluorescence Microscopy. *J Trauma* 1997; 43: 813-819.
6. Glatter RD, Goldberg JS, Schomacker KT, Compton CC, Flotte TF, Bua DP, Greaves KS, Nishioka NS, Sheridan RL. Carbon Dioxide Laser Ablation with Immediate Autografting in a Full Thickness Porcine Burn Model. *Annals Surg* 1998. In press.
7. Payne BP, Nishioka NS, Mikic BB, Venugopalan V. Comparison of Pulsed Laser Ablation at 10.6 and 9.5  $\mu\text{m}$ . *Lasers Surg Med* 1998; 23: in press
8. Sheridan R, Lydon M, Petras L, Schomacker KT, Glatter RD, Tompkins RL. Laser Ablation of Burns: Initial Human Trial. *Surgery* 1998; Submitted.
9. Jerath MR, Schomacker KT, Nishioka NS. Estimation of the Extent of Burn Injury using Indocyanine Green Fluorescence. *J Trauma* 1998, In Prep.
10. Fike EE, Schomacker KT, Glatter RD, Nishioka NS. Determination of Burn Depth using Laser Speckle in a Porcine Burn Model. In prep.
11. Schomacker KT, Glatter RD, Torri A, Lucchina LC, Bua DP, Greaves KW, Flotte TF, Sheridan RL, Nishioka NS. Tissue reflectance as feedback control in an automater laser debridement system. In prep.

### **Meeting Abstracts:**

1. Jerath MR, Bua DP, Silver GM, Hanel E, Tearney G, Nishioka NS. Fluorescence imaging of iv indocyanine green as a means of gauging burn injury depth. International Society of Optical Engineering Annual Progress in Biomedical Optics Meeting, January 1994, Los Angeles CA; in Advances in Laser and Light Spectroscopy to Diagnose Cancer and Other Diseases, Alfano RR ed., Proc 2135, A34.
2. Kilmer SL, Nishioka NS, Jerath MR, Farinelli WA, Flotte TJ, Anderson RR. Burn depth diagnosis using indocyanine green. American Society for Laser Medicine and Surgery fourteenth Annual Meeting, April 1994, Toronto Ontario; Lasers Surg Med 1994, Suppl 6, A262.
3. Lucchina LC, Bua DP, Domankevitz Y, Silver GM, Sheridan RL, Nishioka NS. High-power CO<sub>2</sub> laser ablation and split thickness grafting of burn wounds. Society for Investigative Dermatology, April 1994; J Invest Dermatol 1994; 102: 602(A471).
4. Sadhwani AG, Schomacker KT, Tearney GJ, Nishioka NS. Estimate of burn eschar thickness by Analysis of near field speckle. American Society for Laser Medicine and Surgery Fifteenth Annual Meeting, April 1995, San Diego CA; Laser Surg Med 1995; Suppl 7: A9.
5. Kilmer SL, Sandison D, Schomacker KT, Anderson RR, Nishioka NS. Update on burn depth diagnosis using indocyanine green. American Society for Laser Medicine and Surgery Fifteenth Annual Meeting, April 1995, San Diego CA; Lasers Surg Med 1995, Suppl 7, A228.
6. Sheridan RL, Schomacker KT, Lucchina LC, Hurley J, Torri A, Greaves KW, Tompkins RG, Nishioka NS, Parrish JA. Burn depth estimation using indocyanine green fluorescence: Initial human trial. Twenty-seventh Annual American Burn Association Meeting, April 1995, Albuquerque NM, A218p.
7. Schomacker KT, Torri A, Lucchina LC, Flotte TF, Sheridan RL, Nishioka NS. Tissue reflectance as feedback control in an automater laser debridement system. Twenty-eighth Annual American Burn Association Meeting, April 1996, Nashville TN, A97.
8. Schomacker KT, Torri A, Sandison DR, Nishioka NS, Sheridan RL. Biodistribution of indocyanine green in a porcine burn model. Twenty-eighth Annual American Burn Association Meeting, April 1996, Nashville TN, A99.
9. Goldberg JS, Schomacker KT, Compton CC, Nishioka NS, Sheridan RL. Skin grafting following CO<sub>2</sub> laser debridement of full-thickness burns in porcine model. Twenty-ninth Annual American Burn Association Meeting, April 1997, New York NY; Burn Care Rehabil 1997; 18(part 3): S153(A166).
10. Glatter RD, Schomacker KT, Bua DP, Greaves KW, Nishioka NS, Sheridan RL. Technical development of a rapidly-scanned quasi-continuous wave CO<sub>2</sub> laser for burn debridement. Twenty-ninth Annual American Burn Association Meeting, April 1997, New York NY; Burn Care Rehabil 1997; 18(part 3): S190(A240).
11. Sheridan RL, Lydon M, Petris L, Schomacker K, Glatter R. Initial human trial of laser ablation of burn eschar. Thirtieth Annual American Burn Association Meeting, April 1998, Chicago IL; Burn Care Rehabil 1998; 19(part 2): S204(A138).

## APPENDIX A

### *Wellman Laboratories of Photomedicine*

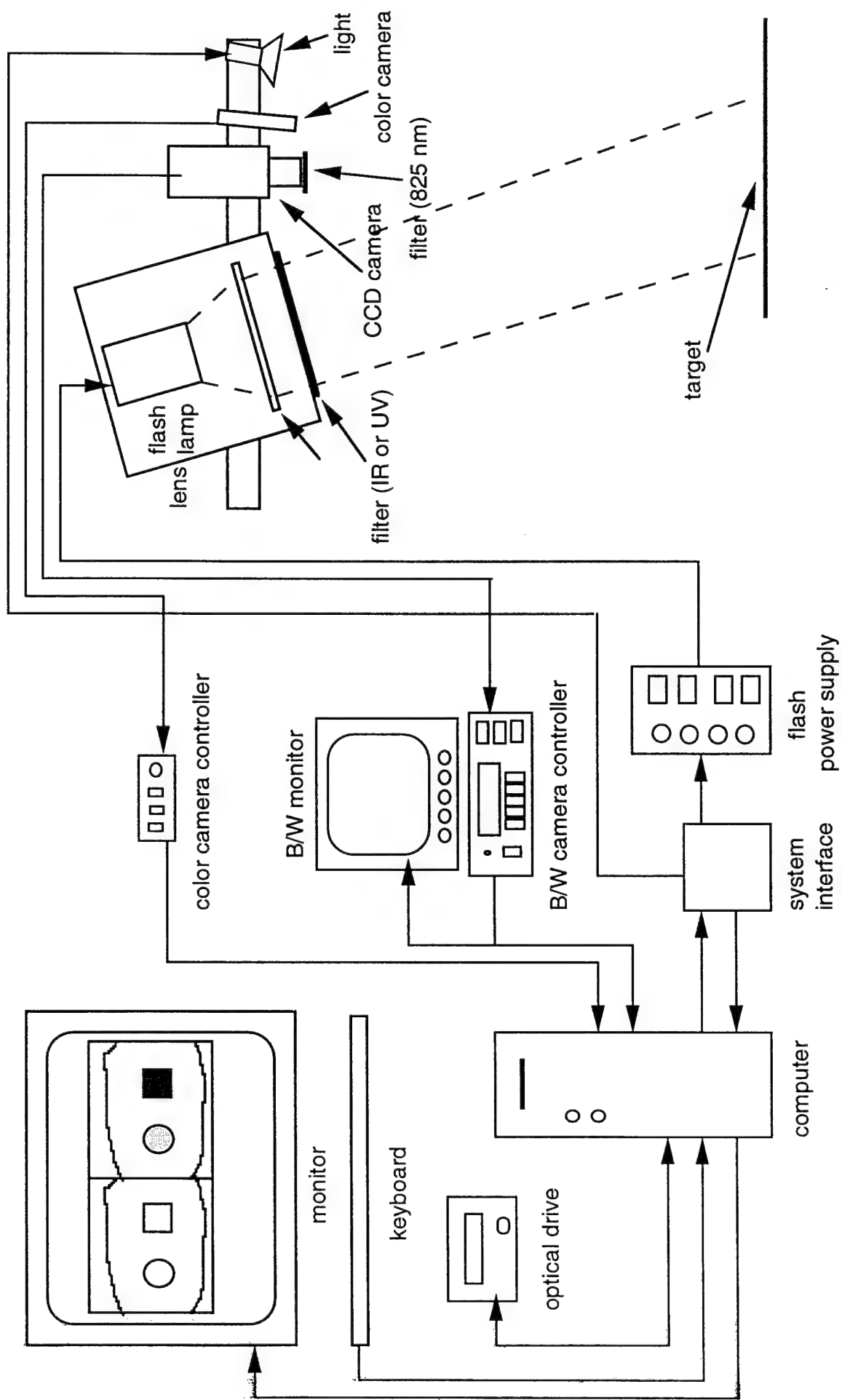


### **Burn Diagnostic System**

## SYSTEM PARTS LIST

Macintosh Computer	Quadra 900
Perceptics Corp. Frame Grabber	112291 REV-3.0
Raster Ops Video Board	0002-0249 REV-C1
National Instruments I/O Board	NB-MIO-16
Raster Ops RGB Video Monitor	GDM-1935
Dage MTI B/W CCD Camera	CCD-C72
Elmo Color CCD Camera	MN401E
Panasonic B/W Video Monitor	TR-930
RICOH Optical Disk Drive	RS-9200EX
International Light Radiometer	IL1700
International Light Detector	SED 623
Staco Isolation Transformer	ISO12020LC
Magnetic Electromotren Lift	HC 8AWAK2-005
Speedotron Flash	2405
IR Light Filter, Excitation	780BP10
UV Light Filter, Excitation	400BP10
Camera Filter	825BP20
MWK Ind's. Laser Diodes	LD67N-3
System Electronic Interface	Wellman Labs Design
Fresnel Lens	
60W Incandescent Lamp	





# DIAGNOSTIC SYSTEM BLOCK DIAGRAM

## SYSTEM OPERATION

The Burn Diagnostic System is relatively simple to use and can be operated in a variety of settings. Once the main power is applied, a master On/Off switch will distribute power to all major subassemblies with the exception of the flash lamp power supply. This supply has its own power switch which must be engaged for proper operation. The computer has a secondary power switch that once pressed will initiate a system boot-up procedure. This loads all the required software necessary to control the computer hardware and acquire both color and black & white images.

Upon completion of the system power up, it is necessary to get the Dage CCD system out of Test Mode by pressing the Test button on the control unit. Also, a gain of 125 is required and is selected on the control unit. At this point the system is fully configured to begin an acquisition procedure.

By selecting the BIS\_alias icon, a set of software routines are initiated to begin image acquisition. A screen will appear that is used to display both color and fluorescence images and also select desired operation. Select NEW to input the patient's name, folder, and any comments. Once all this information is entered select OK and the screen will display the live color video image. This allows for target alignment and height adjustment. Two HeNe laser diodes are mounted so that when their spots overlap on the target the height of the system is correct. The height adjustment is achieved by pressing the Up or Down button of the power lift arm. Also the system arm can be manually adjusted in 3-axis to achieve proper target alignment.

The system is now ready to acquire images selecting CAPTURE to begin this procedure. Once initiated, the system performs automatically requiring no manual intervention. The color image is frozen, the laser diodes are commanded off, and a reflectance image from the CCD-C72 is taken and temporarily stored in RAM disk. The incandescent lamp is turned off and a background image is acquired and temporarily stored prior to acquiring the fluorescence image. The system monitors the flash source power and allows a fluorescence image to be taken only when the flash power is above a set threshold. This guarantees a consistent amount of light energy on target for each fluorescent image acquired. When the monitor state is a go, the flash is triggered at the time the CCD-C72 video signal is at the start of a frame. This frame, containing the fluorescence data, is captured and stored in RAM disk. The image is then displayed on the screen for a quick look. In all, four images are acquired at each target area requiring almost 1.5 megabytes of storage space. When the last image is taken, the laser diodes and incandescent lamp are automatically turned back on to allow easy alignment of the next target area.

The last screen in this sequence will appear after the fluorescent image is completely displayed. An input window will appear to SAVE, GO LIVE, or CANCEL. Selecting SAVE will put all four images into the patient's folder on the hard disk while selecting GO LIVE will delete the images from the temporary storage area. In both cases, the system will return to the live color video screen to acquire another set of images. Selecting CANCEL will allow the entering of a NEW patient folder, name or QUITting.

# BURN DIAGNOSTIC SYSTEM SPECIFICATIONS

## SYSTEM SPECIFICATIONS

Input Voltage	120 VAC
Max. Power (not to exceed)	20 Amps
Target Distance	57.9 cm from Elmo camera lens
	70.1 cm from Dage camera lens
Elmo Camera FOV	11.7x11.6 cm (at target)
Dage Camera FOV	11.3x10.8 cm (at target)
Flash Energy @ 780 nm	1.1 mJ/square cm (at target)

## DAGE CCD-C72 Camera

See the following two pages

## SPEEDOTRON FLASH UNIT

Max. Power	2400 Watt-secs
Recycle Rate	2 Secs
Weight	23 Lbs
Size	6.4x8.8x13 Inches

## IR LIGHT FILTER

Center Frequency	780 nm
Bandwidth	10 nm

## UV LIGHT FILTER

Center Frequency	400 nm
Bandwidth	10 nm

## CCD CAMERA FILTER

Center Frequency	825 nm
Bandwidth	20 nm

## DAGE CCD-C72 Specifications

### ELECTRICAL

Input Voltage	:	105 to 135 volts 50/60 Hz or 210 to 250 volts 50/60 Hz									
Input Power	:	18.5 watts @ 120VAC Line									
Vertical Sweep Rate	:	CCD-C72: 59.94 Hz Standard									
Horizontal Sweep Rate	:	CCD-C72: 15,734 Hz Standard									
Scanning	:	CCD-C72: 525/60 Crystal Controlled									
Type of Sync and Blanking Waveform	:	CCD-C72: EIA RS-170A									
Pick up Device	:	Interline Transfer CCD									
Pick up Area	:	8.8mm X 6.6mm									
Active Picture Elements	:	CCD-C72: 768(H) X 493(V)									
Picture Element Size	:	CCD-C72: 11um(H) X 13um(V)									
Pixel Clock Output Frequency	:	CCD-C72: 14.31818 MHz									
Resolution	:	CCD-C72: Horizontal - 570TVL Picture Elements = 756(H) Vertical - 350TVL									
Sensitivity	:	<table><tr><td></td><td>w/IR Filter</td><td>w/out IR Filter</td></tr><tr><td>Usable Video (20% of full)</td><td>.001fc</td><td>.0004fc</td></tr><tr><td>Full Video</td><td>.002fc</td><td>.001fc</td></tr></table>		w/IR Filter	w/out IR Filter	Usable Video (20% of full)	.001fc	.0004fc	Full Video	.002fc	.001fc
	w/IR Filter	w/out IR Filter									
Usable Video (20% of full)	.001fc	.0004fc									
Full Video	.002fc	.001fc									

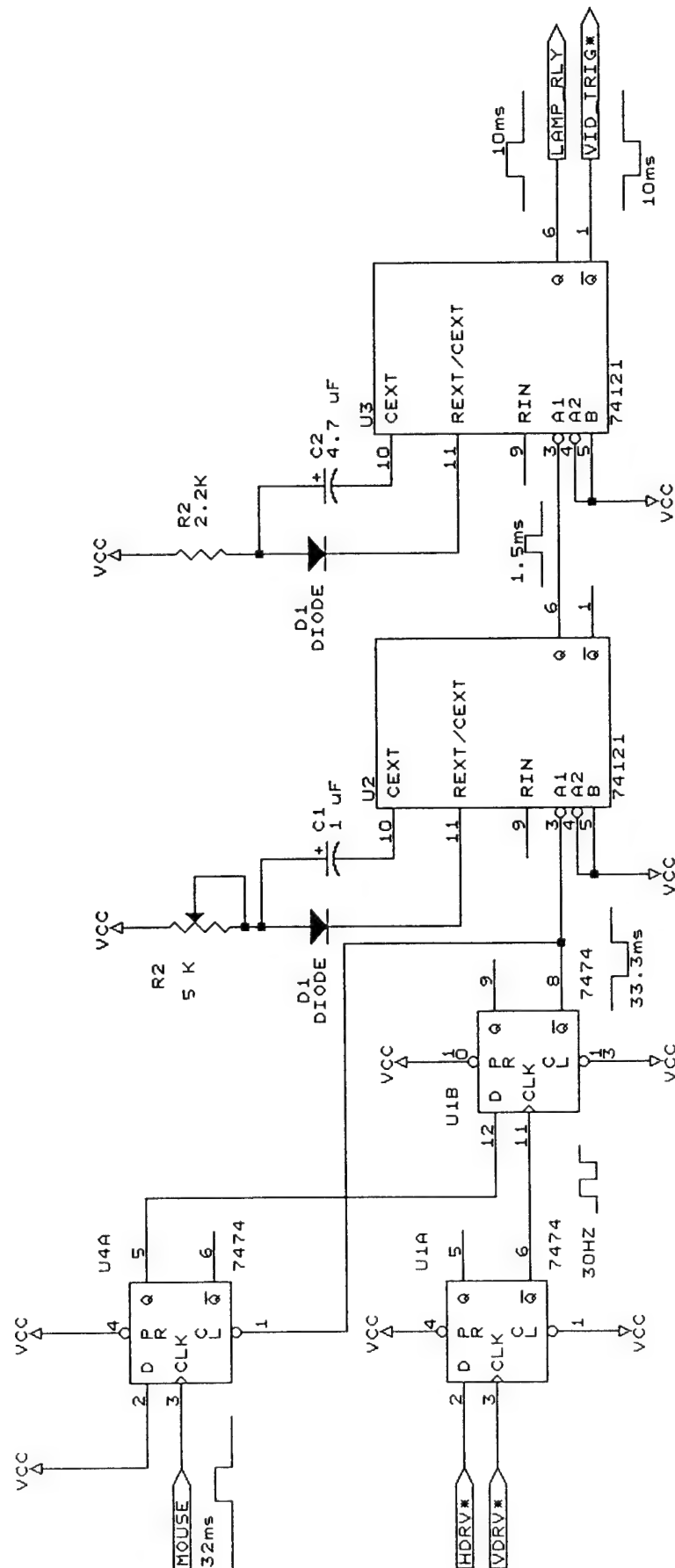
### DAGE CCD-C72 Specifications Continued

Automatic Light Range	:	Faceplate Illumination Versus Video Output Level Change 100:1 with less than 1 db change
Automatic Gain	:	100:1 Peak-Average Adjustable
External Gain Switch Time	:	Less than 5 ms.
Shading	:	Less than 5% overall
Camera Cable	:	8' Superflex Optional Lengths to 50'
Video Output	:	Composite 1Vpp, black to white .65 volts, .3v sync, black negative polarity; source ter- minated 75 ohm output up to 2.5Vpp composite video avail- able.
Video Processor	:	10MHz Flat Response White Clipper Variable Bandwidth Control Automatic Black Level Automatic Video Level Gamma Correction - Switchable
Video Polarity	:	Switchable
Enhancement	:	Adjustable 0 to 12 db at 5.5MHz
Signal to Noise	:	50 db typical (Gamma "OFF", Stretch "OFF", Enhance "MIN", Bandwidth "MIN", Hi/Lo Gain "Lo")
Baud Rate	:	4800 bps

### MECHANICAL

Head (Less Lens)	:	1.2" H, 1.7" W, 4.8" L
Weight	:	6.4 oz., 180 g.
Control Unit	:	3 3/4" H, 8 5/8" W, 12 3/4" L

# SYSTEM INTERFACE - FLASH/VIDEO TRIGGER SCHEMATIC



Drawn By: Ken Greaves  
File: diaglamp.sch

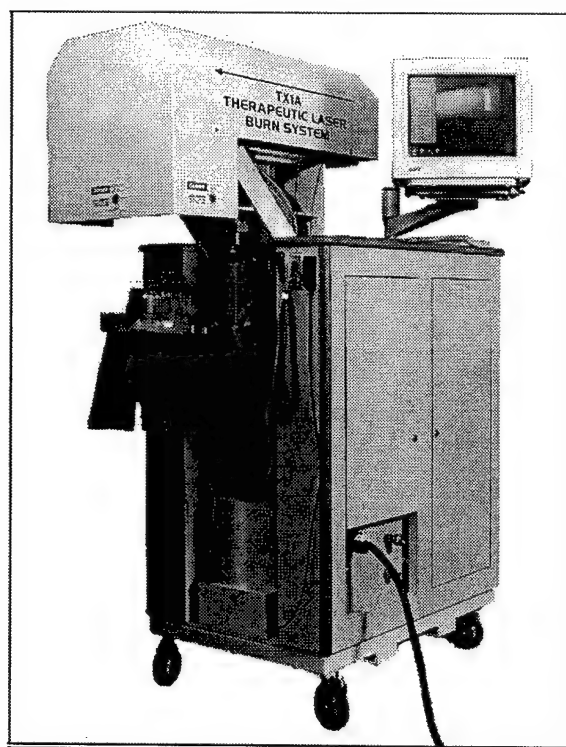
Title  
LAMP CONTROL, BURN IMAGING SYSTEM

Size Document Number  
A

REV  
Date: March 25, 1994 Sheet 1 of 1

## APPENDIX B

### *Wellman Laboratories of Photomedicine*



### **Burn Therapeutic Laser System**

## **Major Components**

Coherent Diamond 64, 150 watt RF excited water cooled CO<sub>2</sub> Laser

Digital Celebrity XL 590 computer.

General Scanning X-Y scanning system

Mapoptics Optical Storage device

Coherent Field Master 1000 watt Power meter

Laser Precision Universal Power Meter

Elmo Color camera

Memorex 8mm Video Cassette Recorder

Sony PVM-1350 video monitor, remote

Buffalo Filter 1200 Smoke Evacuator

lift Magnetic Corp. HC 8AWAS2u-0005

Newport Optical with optical components.

Custom Enclosure



## System Specifications

Laser power ~150 watts at target sight

Energy per pulse 35 J/cm<sup>2</sup>

Spot Size 1.5mm ( 750mm FL ZnSe lens)

Depth of field +/- 2 in.

Scan speed and dwell time adjustable to give the proper energy at the target sight.

Distance to target 26 in. measured from last scanning mirror adjustable via the power lift.

Maximum target area 8 in. X 8 in.

Built in water cooled power meter capable of > 500 w

Green diode pointing laser aligned coaxial to the CO<sub>2</sub> Laser

Red diode laser (s) adjusted to cross at the focal point. ( focusing method).

Doctors interface would allow burn surgeon to enter patient information, system operating parameters, and select area of debridement. A smoke removal system and target area enclosure is included as apart of the overall system.

TX1A Weight 860 lbs.

The system has the following safety features:

Redundant hand switches for surgeon and assistant that will terminate operation if a problem is recognized by either person.

Instrument monitoring electronics was designed to insure all components are operating properly and to terminates the procedure if a fault is identified.

The system also measures room temperature, humidity, and input/output water temperature.

## **System Operation**

### **Preliminary Checks**

Connect the main power cord 208 vac 3 phase 30 amp to the source.

Connect the secondary power cord 115 vac 1 phase 30 amp to the source.

Connect the coolant water lines via the quick disconnect to the filtered water source and the drain (1.5 gal/min).

Place the smoke evacuator in the appropriate position (typically on the right side as viewed from the laser output end). Plug the evacuator into 115 vac 15 amp line and connect the control cable to the foot switch inlet.

Turn ON the 3 phase breaker and the three plug strips located behind the door above the power and water connectors.

Strip marked phase A Powers the; Audio Mixer/Amp, VME Chassis, Universal Radiometer, and Camera Control Unit.

Strip marked phase B Powers green and red pointing and focusing diodes respectively, Coherent Field Master Power Meter, white light, and power lift.

Strip marked phase C Computer/Monitor, Optical Disk Drive, Hi 8 recorder.

When the computer is fully functional, as denoted by the appearance of the doctors interface screen, check the logic monitor LED's (with the exception of the smoke evacuator LED's). All the LED should be illuminated indicating all major electronic components are activated. The smoke evacuator can be tested by pressing the button on the green hand piece. The smoke evacuator LED will light and go out when released which will then trigger the delay circuit causing the

smoke evacuator to stay on for a predetermined period of time as indicated by the smoke evacuator **Delay ON LED**.

The delay time can be set from the switch on top of the box marked Smoke Evacuator Electronic Delay Box. located behind the door above the power input cables. The delay period can be set for zero, 3,5,10, 25 seconds or infinity. Zero seconds being fully counter clockwise. Test of the optical lift which is used for focusing the laser above the target area should be performed. The up/down buttons are located on the right side of the enclosure facing the system from the doctors point of view. A final check of all the panel fault indicator light should be made. These fault indicator lights are located on the TX1A front panel, General Scanning driver electronics, Coherent remote box, Coherent fault monitor box.

At this point all the electronics and monitoring devices are operational, and the main laser green power button located on the left side of the front panel can now be actuated. The green light just to the left of the green power button will remain on if the power is successfully actuated.

Please note to the right of the green ON button is the **red Off button**. To the far right is the location of the **LARGE RED Emergency OFF button**. The Emergency Off button will disable the total system should an emergency arise requiring it's actuation. Also located on the front panel is the relative humidity and temperature digital display. This system can be operated in temperatures and humidity not to exceed 90 degree and 90 % respectively, provided dry nitrogen purge gas is used to continuously flush the system. Take note to insure the scanner mirrors are up to operating temperature. The General Scanning X-Y driver boards have an indicator light that will be illuminated when the proper temperature is reached.

### **Turn on Procedure**

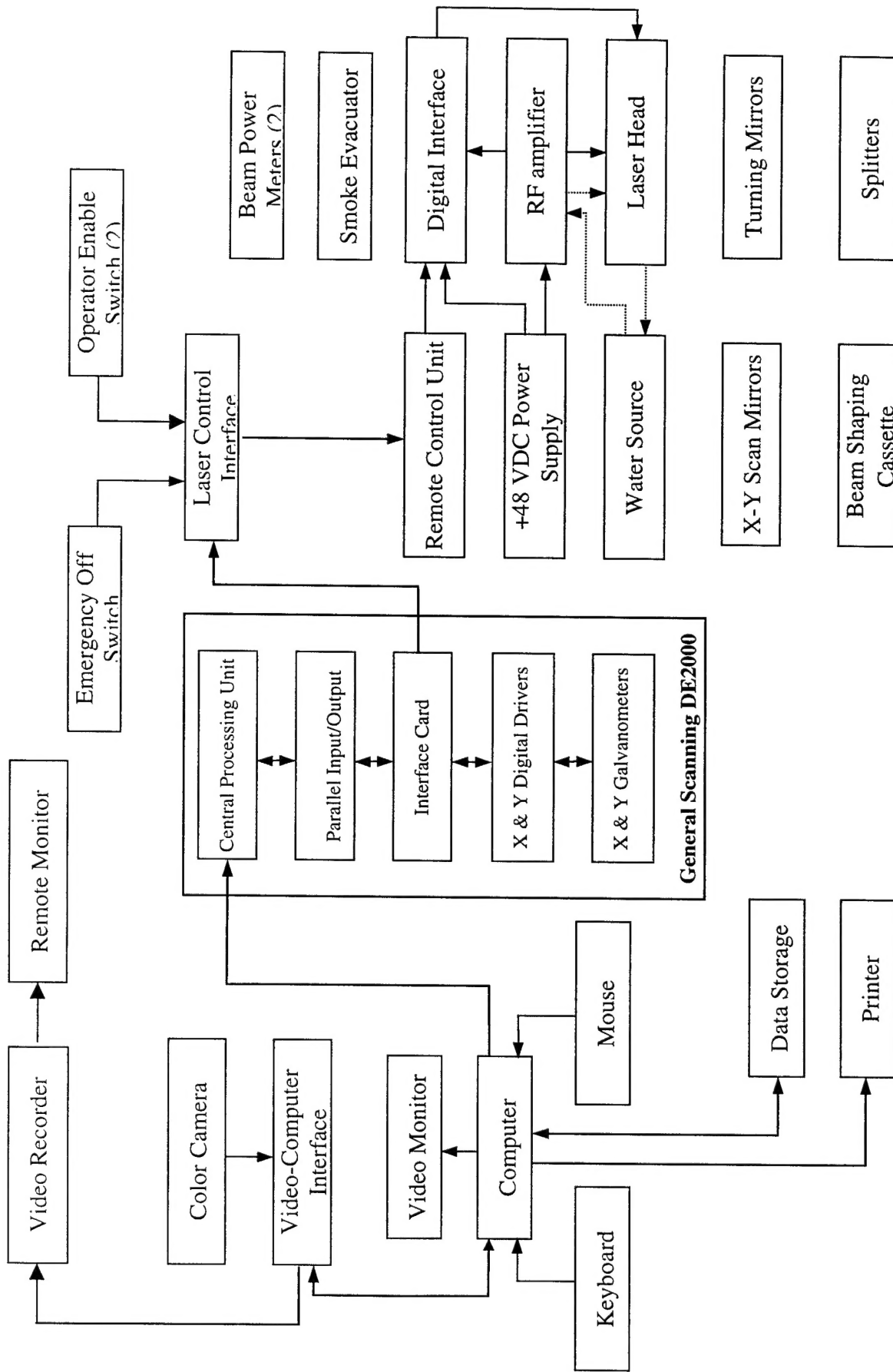
The TX1A Laser Debridement Burn System is now ready to be operated for the desired procedure. This is the appropriate time to enter system parameters and patient information. Place the target test piece under the laser delivery end, adjust the lift height using the up/down lift buttons so the red laser diode spots are superimposed on each other. The CO<sub>2</sub> laser is now focused for the proper distance at the target. The target test piece can be a black anodized aluminum square with a 5cm by 5cm carefully scribed mark. This mark will be used to demonstrate the accuracy and pointing capability of the scanning system. Observe the target and outline the 5X5cm area. The outline can be accomplished by first using the mouse to place the cursor over the still window of the doctors interface screen Fig.4. Click the left button twice, once to bring the window forward and the second time to actuate the capture of the picture. Position the cursor on the captured picture and click the left button twice, once to bring the picture forward and the second time to mark the initial point. Drag the cursor to the second point and click the left button. Continue this until you have the area of interest enclosed. When you have completed the area you wish to capture click the middle button. This will enclose the area you wish to ablate.

**Note Do not cross the marked lines over itself, an error will result.**

The next step is to outline the area you just enclosed by bringing the cursor to the button marked outline (doctor's interface screen). Press the mouse left button twice. The first time to bring the screen forward and the second time to outline the target. Watch the target or the live monitor. The green laser should outline the area you enclosed. To insure the scan area is correct one should scan the outline area with the green laser. To accomplish this, first set the remote shutter switch on the remote control unit to local, and set the shutter switch to closed. Closing the shutter will prevent an accident by eliminating CO<sub>2</sub> laser light from exiting the laser head.

Take the mouse and position the cursor on the button marked **laser warm up** and actuate this button then press the arm button. The arm button will light red Fig 6. Press and hold the green button on the hand switch this will actuate the smoke evacuator (this should be done by the nurse/technician). When the doctor is ready, he/she, can then press and hold

the red button (doctor's hand switch), this will actuate the scan process. The doctor and assistant should view the target directly or on the monitor screen to be assured the ablation area is sighted correctly and the speed /ablation time is within specs. ***NOTE*** *If the outline of the targeted area is not acceptable (X-Y offset, size, or rotation) a complete calibration will have to be performed. See section on calibration.* The next recommended test is the **weight loss go, no-go test**. A 2" x 2" x 1/8" Plexiglas piece should be weighed and the value recorded. Repeat the prior procedure we used on the black anodized aluminum outlined **5cm X 5cm** scribed mark. The Plexiglas piece is then placed in the target area. Complete the focusing procedure using the red diode lasers. Before operating the laser make sure the correct system parameters are set. The laser pulse width and period can be set by adjusting the thumb switches located on the laser Remote Control Unit Fig 7. These values are 166 microseconds (6024 hertz) and 82 microseconds respectively. ***(NOTE do not exceed a 50 % duty cycle and/or operate at 5000 hertz).*** With the remote shutter placed in remote, actuate the laser warm up button on the doctor's interface screen using the cursor Fig 4 . Press the measure power button using the cursor and record the value in the window marked laser power of the **system parameter sub screen**. The laser powder off button on the interface screen should then be actuated. *(For a more in depth description of the Diamond 64 operation refer to the Diamond 64 Manual.)* Close this sub screen and enter the number of passes on the screen marked passes. After you have weighed the plastic go-no-go test sample, place it in the same target area where the black anodize piece was. Focus the plastic sample with the red diode lasers. Repeat the outline target to insure the target area is addressed correctly. Measure the laser power again and enter this value if it is different. . The next step is to complete the laser scan using the same procedure as we used with the green laser including the use of the smoke evacuator. For the go- no-go test, I would recommend utilizing the wan. The smoke enclosure however can be used if you so desire. When the scan is completed the Plexiglas test piece weight is re-measured and compared to the original measurement prior to laser scanning. The weight loss should be approximately 0.5 grams to pass the go-no-go test. The weight loss of 0.5 grams is achieve with an energy at target of 35 J/cm<sup>2</sup>. The system is now ready for laser ablation of tissue, animal and or human.



## Automated Laser System for Burn Therapy